Polymer Flow in Porous Media

Arne Skauge(1,3)*, Nematollah Zamani(2), Jørgen G. Jacobsen(1,2), Behruz S. Shiran(2), Badar Al-Shakry(1), and Tormod Skauge(3)

1. Dept. of Chemistry, Allegaten 41, University of Bergen, N-5020 Bergen, Norway
2. Uni Research, N-5020, Bergen, Norway
3. Energy Research Norway, N-5020, Bergen, Norway
* Correspondence: arne.skauge@kj.uib.no, Tel: 47-5558-3358

Abstract

Polymer flooding is one of the most successful chemical EOR methods, and is primarily implemented to accelerate oil production by sweep improvement. However, other benefits have extended the utility of polymers. During the last decade, it has been evaluated for an increasing number of fields, both offshore and onshore. This is a consequence of improved polymer properties, which extends the use to HTHS (high temperature high salinity) conditions and of improved understanding of flow mechanisms such as for heavy oil mobilization.

A key issue in understanding polymer performance is to control and predict in-situ porous medium rheology. The first part of this paper reviews recent developments in understanding polymer flow in porous medium. Especially, polymer in-situ rheology and injectivity is discussed.

The second part of this paper reports polymer flow experiments using the most applied polymer for EOR processes, HPAM (partially hydrolyzed polyacrylamide). The experiments address high rate near-wellbore behavior (radial flow) as well as reservoir rate steady state flow (linear flow) and discuss differences observed in terms of flow conditions. In addition, impact of oil on polymer rheology was investigated, and compared to single-phase polymer flow in Bentheimer sandstone rock material. Presence of oil leads to a reduction in apparent viscosity.

1. Introduction

Success of polymer flooding depends on injected solutions ability to transport polymer molecules deep into the reservoir, and thus provide enhanced mobility ratio conditions for the displacement process. In the following sections, we will focus on principal parameters, crucial in the decision-making process for satisfactory polymer flood design.

Application of polymer flooding in tertiary oil recovery may induce high injection pressures, resulting in injectivity impairment. Since volumetric injection rate during polymer flooding is constrained by formation fracture pressure, project economics may be significantly affected. Thus, injectivity is a critical parameter and key risk factor for implementation of polymer flood projects.

A large number of injectivity studies, both theoretical and experimental, has been performed in porous media during recent decades, albeit mainly studies of linear cores in absence of residual

oil [1-7]. Recently, Skauge et al. [8] performed radial injectivity experiments showing significant reduction in differential pressure compared to linear core floods. This discrepancy between polymer flow in linear cores versus radial discs were partly explained in terms of differing pressure conditions, where polymer molecules are exposed to transient and semi-transient pressure conditions in radial discs, as opposed to steady state conditions experienced in linear core floods. In addition, they observed that onset of shear thickening occurs at significantly higher flux in radial floods. Based on these results, injectivity is suggested to be underestimated from experiments performed in linear core plugs. However, these experiments were performed in absence of residual oil. If residual oil has a significant effect on polymer propagation in porous media, experiments performed in absence of residual will not be able to predict polymer performance accurately.

Experimental studies investigating effects of residual oil on polymer propagation through porous media are sparse, although they generally show decreasing levels of polymer retention in presence of residual oil [9-10].

History matches performed in this paper aim to illuminate injectivity of partially hydrolyzed polyacrylamides (HPAM) in radial discs saturated with residual oil, as these conditions best mimic actual flow conditions in oil reservoirs. Results show that presence of residual oil reduces apparent viscosity of HPAM in flow through porous media, thus improving injectivity. These results may facilitate an increase in polymer EOR project implementation, as previous ones deemed infeasible may become economically viable.

2. Theory

2.1 In-situ rheology

Polymer viscosity as a function of shear rate may be measured using a rheometer. During the measurement process, polymer solutions will be exposed to different shear rates in a stepwise manner. For each shear rate, polymer viscosity is measured after steady state conditions are achieved, and is referred to as bulk viscosity. However, polymer molecules experience significantly different flow conditions in rheometers compared to porous media:

(I) unlike rheometers, porous media exhibits an inherently complex geometry,

(II) phenomena such as mechanical degradation may change rheological properties,

(III) although they only demonstrate shear thinning behavior in rheometers, polymer solutions may exhibit shear thickening behavior above a certain critical flow rate,

(IV) due to tortuosity of porous media and existence of several contraction-expansion channels, polymer solutions will be exposed to a wide range of shear rates at each flow rate, resulting in significantly different rheology behavior compared to bulk flow.

To account for these contrasting flow conditions, in-situ viscosity has been suggested to describe fluid flow behavior of polymer solutions in porous media. In-situ viscosity is a

Peer-reviewed version available at Colloids Interfaces 2018, 2, 27; doi:10.3390/colloids2030027

macroscopic parameter that can be calculated using Darcy's law for single-phase non-Newtonian fluids:

$$\mu_{app} = \frac{KA}{Q}\frac{\Delta P}{L} \tag{1}$$

It is generally measured in core flood experiments as a function of Darcy velocity. Comparison of in-situ and bulk rheology (Figure 1) shows vertical and horizontal shifts between viscosity curves. Vertical shifts may be due to phenomena such as mechanical degradation, while horizontal shifts is due to a conversion factor between in-situ shear rate and Darcy velocity, shown as α.

Due to the time consuming nature of in-situ measurements, there have been several attempts to investigate in-situ rheology, both analytically and numerically. In spite of extensive studies [11-19], limited success has been achieved to reliably relate in-situ to bulk viscosity based on polymer solution and porous media properties. Most of these models have been developed based on analytical solutions of non-Newtonian flow through capillary bundles, which simplifies the complex geometry of porous media.

In the following, calculation procedure of in-situ viscosity is briefly explained:

1. Analytical solution for a power-law fluid ($\mu = C\,\dot{\gamma}^{n-1}$) at a given flow rate through a capillary tube with an arbitrary radius (R) can be defined by eq. 2. By comparing eq. 2 with Poiseuilles volumetric flow rate for Newtonian fluids in a tube (eq. 3), an apparent viscosity and shear rate can be obtained by eq. 4 and eq. 5, respectively.

2. The analytical equation in a single tube (eq. 5) can be extended to account for real porous media by using capillary bundle approach [20-22]. An equivalent radius of capillary bundle model for porous media with known porosity (φ), permeability (K) and tortuosity (ψ) can be obtained by eq. 6. By calculating Darcy velocity and substituting equivalent radius (eq. 6) into eq. 5, apparent shear rate as a function of Darcy velocity can be obtained by eq. 7.

$$Q = \frac{\pi n}{3n+1}\left(\frac{\Delta P}{2CL}\right)^{1/n} R^{\frac{3n+1}{n}} \tag{2}$$

$$Q = \frac{\pi}{8\mu}\frac{\Delta P}{L} R^4 \tag{3}$$

$$\mu_{eff} = C\left(\frac{3n+1}{4n}\right)\left(\frac{R\Delta P}{2CL}\right)^{\frac{n-1}{n}} \tag{4}$$

Peer-reviewed version available at Colloids Interfaces 2018, 2, 27; doi:10.3390/colloids2030027

$$\mu_{app} = C\,\dot{\gamma}_{app}^{n-1} \Rightarrow \dot{\gamma}_{app} = \left(\frac{3n+1}{4n}\right)^{\frac{1}{n-1}} \left(\frac{R\Delta P}{2CL}\right)^{1/n} \quad (5)$$

$$R_{eq} = \sqrt{\frac{8K\psi}{\phi}} \quad (6)$$

$$\dot{\gamma}_{app} = 4\left(\frac{3n+1}{4n}\right)^{\frac{n}{n-1}} \frac{U}{\sqrt{8K\phi\psi}} \quad (7)$$

3. The above expressions are considered as analytical basis for calculating apparent viscosity in porous media. Based on eq. 7, a simplified linear correlation is generally suggested between apparent shear rate and Darcy velocity, i.e. Eq. 8, in which correction factor (α) is the key issue. Some proposed equations for correction factor are summarized in Table 1. By comparing different coefficients, different values for apparent viscosity may be obtained.

$$\dot{\gamma}_{app} = \alpha \frac{U}{\sqrt{K\phi}} \quad (8)$$

Based on capillary bundle approach, other models are also proposed by Bird et al. [23], Christopher and Middleman [24], Teeuw and Hesselink [15], in which the modified Blake-Kozeny model is used for power-law fluids (eq. 9) and apparent viscosity is obtained using eq. 10.

$$U = \left(\frac{K}{\mu_{app}}\frac{\Delta P}{L}\right)^{1/n} \quad (9)$$

$$\mu_{app} = C\left(\frac{3n+1}{4n}\right)^{n}\left(\frac{K\phi}{\beta}\right)^{(1-n)/2} \quad (10)$$

Based on the discussion between Teeuw and Hesselink [15], tortuosity has a dual effect on both shear rate and shear stress calculations. Christopher and Middleman [24] only imported tortuosity in shear stress calculations, while Bird et al. [47] imported tortuosity into the shear rate term. Various values of β chosen by different authors are summarized in Table 2.

Hirasaki and Pope [25] conducted several core flood experiments where permeability was in the range of 7-23 mD, porosity in the range of 18-20% and residual oil between 20-32%. Based on these experiments, they concluded that apparent viscosity might be calculated using capillary bundle approach and Blake-Kozeny model as follows:

Preprints (www.preprints.org) | NOT PEER-REVIEWED | Posted: 1 June 2018 doi:10.20944/preprints201806.0015.v1

Peer-reviewed version available at Colloids Interfaces 2018, 2, 27; doi:10.3390/colloids2030027

$$\mu_{app} = HU^{n-1} \tag{11}$$

Where:

$$H = \frac{C}{12}\left(\frac{9n+3}{n}\right)^{n}(150K\phi)^{\frac{1-n}{2}} \tag{12}$$

They also included pore size distribution in their calculations:

$$\mu_{app} = \frac{C}{4}\left(\frac{1+3n}{n}\right)^{n}\frac{\int_0^\infty \sigma(R)R^2dR}{\left[\int_0^\infty \sigma(R)R^{\frac{1+n}{n}}dR\right]^{n}}\left(\frac{q}{\phi}\right)^{n-1} \tag{13}$$

Sadowski and Bird [14] used the Ellis model to obtain viscosity from shear rate. The following equations for apparent viscosity was suggested based on Blake-Kozeny model and capillary bundle approach:

$$\frac{1}{\mu_{eff}} = \frac{1}{\mu_0}\left(1+\frac{4}{n+3}\left[\frac{\tau_{RH}}{\tau_{1/2}}\right]^{n-1}\right) \tag{14}$$

$$\tau_{Rh} = \left(\frac{\Delta P}{L}\right)\left[\frac{D_p\phi}{6(1-\phi)}\right] \tag{15}$$

In the above expressions, μ_0, $\tau_{1/2}$ and n are Ellis model parameters that can be measured in rheometers. By applying these equations, they obtained an acceptable match between experimental and predicted results for low to medium molecular weight polymers.

In summary, none of the proposed models for non-Newtonian fluids in porous media based on capillary bundle approach is in agreement with all experimental results. Therefore, some known limitations of capillary bundle approach are given as follows:

- Neglects complex features of porous media such as tortuosity and pore size distribution.
- Assume unidirectional flow as it neglects interconnectivity between pores.
- Cannot be representative for flow in an anisotropic medium due to its assumption of unique permeability along propagation direction.
- Assume a single radius along bundles with no variation in cross sectional area. Contraction-expansion feature of non-Newtonian flow in porous media is of high importance, especially when studying extensional viscosity, yield stress and elasticity.

Preprints (www.preprints.org) | NOT PEER-REVIEWED | Posted: 1 June 2018 doi:10.20944/preprints201806.0015.v1

Peer-reviewed version available at Colloids Interfaces 2018, 2, 27; doi:10.3390/colloids2030027

- Capillary bundle approach is generally developed based on rheological models in which analytical solutions for velocity profiles is available (e.g. power law and Ellis model). Analytical solutions for some models (e.g. Carreau model) are quite difficult and equation for velocity is implicit (eq. 10 for Carreau model) and needs to be solved iteratively.

$$\frac{\partial v_z}{\partial r} = -\frac{\Delta p\, r}{2L}\left\{\mu_\infty + \frac{\mu_\infty - \mu_0}{\left[1+\left(\lambda\frac{\partial v_z}{\partial r}\right)^2\right]^{\frac{n-1}{2}}}\right\} \quad (16)$$

Duda et al. [26] studied polymer solution rheology inside porous media and reported greater pressure drops experimentally than predicated pressure drops by capillary bundle models, especially at lower values of Carreau power index. Based on their study, a key issue in underestimating correction factors using capillary bundle approach is the weakness of this model to capture interconnectivity of pores and non-uniform cross sections of pore bodies and pore throats (i.e. abrupt contractions and expansions, which is also known as aspect ratio).

According to aforementioned limitations of capillary bundle approach and lack of a universally accepted equation for calculating shear rates in porous media, effective medium theory was eventually suggested. This method was able to remediate certain weaknesses in capillary bundle approach such as pore interconnectivity and variation in cross sections. Canella et al. [16] extended this method to account for power-law fluids in porous media. Core floods was conducted using Xanthan in the concentration range of 300-1600ppm, rock lithology (sandstone and carbonates) in the permeability range of 40-800 mD and various oil residuals (0-29%). Their general assumption was that bulk rheological properties of polymer solutions obeys the power-law model, and suggested the following equation for relation between shear rate and Darcy velocity based on effective medium theory:

$$\dot{\gamma}_{app} = \beta\left(\frac{3n+1}{4n}\right)^{\frac{n}{n-1}}\frac{q}{\sqrt{K\phi S_w}} \quad (17)$$

By using constant value of 6 for β, Canella et al. achieved a satisfactory match with their experimental results, although this value far exceeds correction factors suggested by other researchers [41,47,48]. Even though all published results in the literature is not covered by using this correction factor, better agreement between analytical and experimental results were obtained, such as experiments performed by Teeuw and Hesselink [15] and Gogarty [27].

Canella et al. [16] demonstrated that apparent viscosity depends on both microscopic (connectivity, pore size distribution) and macroscopic properties (permeability, porosity) of porous media. Despite of calculation improvements, neither effective medium theory nor

capillary bundle model are able to estimate correction factor accurately. The great discrepancy of results obtained by models described above and wide range of correction factors suggested [17] confirms that a universally accepted model does not yet exist. Insufficiency of these models to predict in-situ viscosity may be attributed to their lack of incorporating time dependence and using oversimplified porous media models (e.g. capillary bundle).

To avoid over-simplification of porous media obtained by using capillary bundle approach, pore network modelling has been suggested. In contrast to capillary bundle approach, pore network modeling envisage porous media as interconnected bundles with idealized geometries where larger pores (pore bodies) are connected via smaller ones (pore throats). Pore network models have been used to study non-Newtonian fluids that exhibit shear thinning properties by several authors [18, 29-31]. Lopez et al. [18] applied a pore network model to study non-Newtonian fluids using the same approach as for Newtonian fluids, except that viscosity in each bundle was not assumed to be constant and considered as a function of pressure drop. Therefore, an iterative approach was suggested to calculate pressure drop and apparent viscosity. Although they obtained satisfactory agreement between analytical and experimental results using this approach, Balhoff and Thompson [29] stated that effects of concentration was neglected, and consequently proposed a new model based on CFD calculations to include effects of concentration in calculating conductivity of pore throats. They used pore network modeling to model shear thinning polymer flow with yield stress within sand-pack.

Zamani et al. (2017) [28] studied effects of rock microstructures on in-situ rheology using digital rock physics and reported that microscopic properties such as aspect ratio, coordination number and tortuosity may affect deviation of in-situ from bulk rheology.

In some experiments, [22, 26, 27, 32], in-situ rheology relationship has been reported to deviate significantly from behavior in bulk flow. Thereby, in-situ rheology may not be calculated directly from bulk rheology using previously mentioned models. To achieve this, one may use approaches assuming that either in-situ rheological properties are different from bulk rheological properties (e.g. Hejri et al. [32]) or that relation between apparent shear rate and Darcy velocity is non-linear (e.g. Gogarty [27]).

Calculation of in-situ rheology is a controversial subject, and until now, there is no direct method to obtain it. Generally, in-situ rheology is measured by performing core floods. However, Skauge et al. [33] observed significantly different in-situ rheology for HPAM in linear compared radial geometry. This discrepancy might be due to differing pressure regimes and flux conditions experienced by polymer solutions flowing through these inherently different flow geometries.

The problem of in-situ rheology calculations extends beyond finding the appropriate correction/shift factor. It also encompasses predicting onset of extensional viscosity, which is treated as a separate subject in the following section.

Preprints (www.preprints.org) | NOT PEER-REVIEWED | Posted: 1 June 2018 doi:10.20944/preprints201806.0015.v1

Peer-reviewed version available at Colloids Interfaces 2018, 2, 27; doi:10.3390/colloids2030027

2.2 Extensional viscosity

Several experimental results show that, although polymer solutions (e.g. HPAM) only demonstrate shear thinning behavior in a rheometer, it may exhibit shear thickening behavior above a critical shear rate in porous media (Figure 2) [22,26,27,32]. Generally, polymer flow in porous media may be divided into two distinct flow regimes: shear dominant and extensional dominant flow regimes. Since shear thickening occurs in the extensional flow regime, it may also be referred to as extensional viscosity.

Although its source is poorly understood, extensional viscosity is considered as one of the principal aspects of polymer flow in porous media due to its influence on injectivity and oil mobilization. This phenomenon is suggested to be a consequence of elastic properties of polymer solutions (elongational dominated [34] or inertia-dominated flow [35]). Thereby, extensional viscosity is often used interchangeably with elongational viscosity, shear thickening behavior, viscosity enhancement, dilatant behavior and viscoelasticity. Two different models are generally used to explain this phenomenon: (I) Transient network model [36-38] and (II) Coil stretch model [39]. We adhere to the latter of these models.

Polymer molecules may be envisaged as entangled coils, and when exposed to a flow field, two forces may arise: 1) Entropic force that attempt to maintain existing polymer coil configuration. As coil entanglement increase, higher resistance towards deformation is observed. 2) Drag force resulting from interactions between solvent fluid and polymer molecules. When shear rate increases beyond a critical rate, molecule configuration abruptly changes from coil state to stretched state. Therefore, polymer coils start to deform, resulting in anisotropy and stress differences between elongation and compression. Consequently, normal stresses and elastic properties become more dominant.

Choplin and Sabatie [36] suggested that when polymer molecules are exposed to a simple shear flow at a constant shear rate ($\dot{\gamma}$), molecules rotate at a constant angular velocity (ω) proportional to applied shear rate, and in each rotation polymer molecules are stretched and compressed. Time between each rotation may be calculated by eq. 18.

$$t = \frac{\pi}{2} k \dot{\gamma} \tag{18}$$

Where k is a constant of proportionality, related to viscosity. If t is higher than Zimm relaxation time, no dilatant behavior occurs. Consequently, critical shear rate at onset of dilatant behavior may be calculated based on Zimm relaxation time as follows:

$$\lambda_z = \frac{6}{\pi^2} \frac{M_w}{RT} [\mu]_0 \mu_s \tag{19}$$

Preprints (www.preprints.org) | NOT PEER-REVIEWED | Posted: 1 June 2018 doi:10.20944/preprints201806.0015.v1

Peer-reviewed version available at Colloids Interfaces 2018, 2, 27; doi:10.3390/colloids2030027

$$t \le \lambda_z \ , \qquad \dot{\gamma} \ge \gamma^* \xrightarrow{We=\dot{\gamma}\lambda_z} We^* = \lambda_z * \dot{\gamma}^* = \frac{\pi}{2}k \tag{20}$$

Polymer viscosity behavior in extensional flow may be entirely different from its behavior in pure shear flow, i.e. polymer solution may show simultaneous shear thinning and extension thickening behavior. Theoretically, extensional viscosity can be calculated from eq. 21, where N_1 is normal stress difference and $\dot{\epsilon}$ is stretch rate. The relative importance of extensional viscosity and shear viscosity is defined by a dimensionless parameter known as the *Trouton* ratio (eq. 22), initially proposed by Trouton (1906). For non-Newtonian fluids (especially viscoelastic fluids), Trouton's number can reach very large values, such as 10^3-10^4 (i.e. when polymer solution demonstrates shear thinning and extension thickening simultaneously).

$$\mu_e = \frac{N_1}{\dot{\epsilon}} \tag{21}$$

$$Tr = \frac{\mu_e}{\mu_s} \tag{22}$$

In Figure 2, in-situ viscosity of viscoelastic polymers are depicted in both shear and extensional flow regime. At onset of polymer flow, the generated hydrodynamic force from fluid flow (i.e. drag force) is below the threshold value in terms of overcoming entropic forces. Thereby, polymer configuration persists in coil shape and viscosity remains constant and equal to zero shear rate viscosity (upper-Newtonian plateau). As flow rate increases, polymer molecules are exposed to larger drag forces that disentangle polymer coils and aligns them along the flow direction. This coil alignment reduces resistance to flow (i.e. induces viscosity reduction) and is referred to as shear thinning. When polymer molecule orientation is completely aligned, they will start to stretch at increasing flow rates. Change in deformation of polymer molecules may cause normal stress differences. At low stretch rates ($\dot{\epsilon}$), N_1 is very low and by increasing stretch rate, N_1 dramatically increases. In other words, beyond critical shear rate ($\dot{\gamma}_c$), instead of intramolecular interaction, intermolecular interactions will develop which generate amorphous structures much larger than average polymer chain dimensions [41,42].

During extensional flow regime, apparent viscosity generally reaches a maximum value, subsequently followed by a decreasing viscosity interval. This phenomenon may be interpreted as high viscoelastic stresses causing polymer rupture and chain halving, and has been reported as more severe in low permeable porous media [43]. As molecular rupture occurs, new molecular weight distributions emerge (larger molecular weight fractions is distorted) and viscosity behavior of the polymer may be governed by a new molecular weight distribution.

Onset of extensional viscosity, the transition point between shear dominant and extensional dominant flow, depends on polymer, solvent and porous media properties. Effects of polymer properties on extensional viscosity may be investigated by using special rheometers that only

generate pure extensional flow [44-53]. In the following, effects of polymer, solvent and porous media properties on the onset of extensional viscosity are explained.

2.2.1 Polymer concentration: Chauveteau [54] reported that maximum relaxation time increases with polymer concentration, thus dilatant behavior commence at lower shear rate (Figure 3). He also imported effect of concentration into the expression for Zimm relaxation time as follows:

$$\lambda_z = \frac{6}{\pi^2}\mu_s\frac{\mu_{ro}-1}{C}\frac{M_w}{RT} \tag{23}$$

Effect of concentration on extensional viscosity was also investigated by Lewandowska [55]. In contrast to Chauveteau, he reported that dilatant behavior commence at higher shear rate with increasing polymer concentration. He attributed this observation to higher degree of entanglement as concentration increase, thus increasing extent of shear thinning region.

Briscoe et al. [56] could not identify a consistent trend between polymer concentration and onset of extensional viscosity. They assumed that only a narrow region of polymer concentrations are able to generate shear thickening behavior. Below a critical concentration limit, few polymer chains are able to form transient networks. At concentrations above the critical concentration, extent of shear thinning may increase, and consequently onset of shear thickening may be delayed. This effect was also studied by Dupuis et al. [57], where they observed that onset of dilatant behavior decrease with polymer concentration. However, rheological behavior above critical shear rate deviated between different concentration ranges (low: 30-60 ppm, medium: 120-240 ppm and high: 480-960 ppm). Jiang et al. [58] also confirmed scattered data for onset of extensional viscosity as function of polymer concentration. Clarke et al. [59] reported that onset of extensional viscosity is independent of concentration and only depends on molecular weight.

2.2.2 Molecular weight: Length of polymer chains increase with molecular weight, resulting in higher inter and intramolecular entanglement. Thus, extent of shear thinning region will increase and consequently delay onset of dilatant behavior [55]. However, this explanation directly contradicts the expression for Zimm relaxation time (eq. 23), where the latter increase with molecular weight and cause critical shear rate to occur at lower shear rate.

Jiang et al. [58] also studied effects of molecular weight on the onset of extensional viscosity. They concluded that relaxation time increase with molecular weight, thus onset of extensional viscosity occur at lower shear rates. In addition, they observed that this trend was not valid above a critical molecular weight.

Preprints (www.preprints.org) | NOT PEER-REVIEWED | Posted: 1 June 2018 doi:10.20944/preprints201806.0015.v1

Peer-reviewed version available at Colloids Interfaces 2018, 2, 27; doi:10.3390/colloids2030027

Clarke et al. [59] proposed the following correlation for dependency of onset of extensional viscosity on polymer molecular weight:

$$\lambda_{ext} \propto MW^2 C_p^0 \quad (24)$$

2.2.3 Salinity effect: Effect of salinity on polymer rheology may be crucial in some reservoir conditions [82, 83, 86], and depends on polymer type. For typical EOR polymers (e.g. Xanthan, HPAM, or generally non-hydrolyzed polymers) increasing salinity will generally reduce coil gyration and hydrodynamic radius. Due to repulsion between ionic groups in HPAM solutions, increasing salinity will compress electrical double layer on molecular chains and electrostatic repulsion will decrease. In the case of HPAM, reaction mechanism for different metal ions by either monovalent (Na^+) or divalent (Ca^{2+}) cations are different. In the monovalent case, it may suppress the charge effect and reduce hydrodynamic radius. In the divalent case, reactions between cations (i.e. Ca^{2+}) can play role of cross-linkers and influence conformation and rheological properties of HPAM. In both cases, larger shear rates are required to uncoil polymers and shear thickening commence at larger shear rates [56,57,60].

2.2.4 Degree of hydrolysis*:* When HPAM is dissolved in water, electrostatic repulsion forces cause polymer molecules to expand easily and shear thinning region is shortened. Therefore, as degree of hydrolysis increase, onset of shear thickening decrease [55].

2.2.5 Pressure and temperature effect: Although polymers are considered as incompressible fluids, they do exhibit some degree of compressibility. Thus, pressure may have an impact on viscosity. By increasing pressure, free volume between polymer molecules decrease and Brownian motion of polymer chains are inhibited, consequently resulting in viscosity increase of polymer solution. Experimental results [82] indicate that onset of extensional viscosity decrease significantly with pressure.

Effect of temperature on polymer rheology has also been studied extensively [56,58,61,62] and results show that critical shear rate and onset of dilatant behavior are retarded with increasing temperature. This behavior may have the following two explanations. Firstly, polymer relaxation time and solvent viscosity should decrease with increasing temperature, based on eq. 23. Secondly, solvent quality decrease with temperature. By decreasing solvent quality, coil size is reduced and to compensate for this reduction, larger shear rate is needed to uncoil and elongate the polymer. Therefore, onset of extensional viscosity will occur at higher shear rates.

2.2.6 Porous media properties

In addition to polymer properties, porous media may also significantly influence generation of extensional flow, as shown by several experimental [24] and numerical studies [63]. Due to variation in cross sectional area along its propagation path, polymer molecules are forced to

accelerate and deaccelerate. Consequently, they will experience both stretch and shear flow in porous media, and above a critical flow rate, extensional flow will dominate shear flow.

To envisage polymer flow in porous media, the latter may be considered as a simplified contraction-expansion channel. As polymer molecules enter contractions, they will be compressed and stretched. If the flow is below a critical velocity, deformed polymer molecules have sufficient time to return to their original state. Therefore, when polymer solutions enter subsequent contractions, no stress is stored and no additional resistance to flow is observed. However, if polymer relaxation time is high and polymer molecules are not able to return to their equilibrium state between contractions, stress will be stored and accumulated, thus resulting in steep increase in pressure drop and apparent viscosity. This phenomenon can be interpreted as a memory effect of polymer molecules.

Due to inherent nature of porous media, polymer molecules will be sheared near the wall and elongated at the flow axis. Therefore, molecular momentum is transferred by both tangential and normal stress components in porous media. Seeing that polymer molecules are able to rotate in pore space, molecules are not strained and effective viscosity is only controlled by shear. In contrast, if duration of time in which molecules are exposed to strain is sufficient, molecule deformation plays a major role and effective viscosity will be defined by strain [24,63-68].

To predict onset of extensional viscosity in porous media, Deborah number as a dimensionless parameter is defined as a ratio between characteristic relaxation time of a fluid (θ_f) and characteristic time of porous media (θ_p), which is considered as average time to travel from one pore body to another (eq. 25). In other words, Deborah number may be interpreted as the ratio between elastic and viscous forces. Based on this expression, Deborah number is zero for Newtonian fluids and infinity for Hookean elastic solids.

$$N_{De} = \frac{\theta_f}{\theta_p} \tag{25}$$

Polymer solutions may have a wide range of molecular weights that leads to a large number of relaxation times. Many researchers have used the longest relaxation time as representative of θ_f. However, this may cause overestimation of Deborah number at onset of extensional viscosity. Relaxation time may also be calculated from normal stress differences [69].

Some experimental observations revealed that onset of extensional viscosity occurs when N_{De} is larger than 0.5 [70]. However, Deborah number is not constant in different experiments and a wide range of values has been reported. Marshall and Metzner [69] reported Deborah number equal to 0.1 at onset of extensional viscosity, while Chauveteau [54] reported a relatively high Deborah number equal to 10. This wide range of reported Deborah numbers at onset of extensional viscosity is due to difficulty in calculating stretch rate in porous media. To support this idea, Heemskerk et al. [71] reported that by using different polymer types in the same rock sample, critical Deborah numbers (N_{De}) were identical. However, when the same polymer is

used in different rock samples, critical N_{De} varied between 1 and 2. They concluded that measured relaxation time from experimental results can practically help to define onset of extensional viscosity, but suggested equations for stretch rate calculation are not able to capture the exact N_{De} at onset of extensional viscosity. Zamani et al. [66] proposed that to obtain a more accurate estimation of critical N_{De}, stretch rate distribution at the pore scale is required. Metzner et al. [72] concluded that critical Deborah number might only be used as a first estimation of onset of extensional viscosity. In Table 3, some suggested equations for calculation of Deborah number are summarized.

Several experimental results [64,73] show that Deborah number alone is not sufficient to predict onset of extensional viscosity. As an explanation, Ranjbar et al. [74] stated that onset of extensional viscosity highly depends on elastic properties of polymer solutions and relaxation time alone cannot capture viscoelastic properties. Experimental results reported by Garrouch and Gharbi [73] can support this idea. They investigated two different polymer solutions (Xanthan and HPAM) in Berea and sand-packs. Calculated Deborah numbers for these two completely inherently different polymer solutions inside sand-packs were (surprisingly) identical. While Xanthan consist of rigid, rod-like molecules that does not show extensional viscosity, HPAM consist of flexible and elastic chain-structured molecules.

Zamani et al. [63] numerically studied effect of porous media on the onset of extensional viscosity by using real images of porous media obtained from digital rock physics. They confirmed that microscopic features of porous media have significant impact on the onset of extensional viscosity. Furthermore, by increasing aspect ratio and inaccessible pore volume and decreasing coordination number, extensional viscosity occurs at lower shear rates, in agreement with several experimental results [54,64,75].

Skauge et al. [33] reported that in radial flow, onset of extensional viscosity occurs at higher shear rates than at typical core flooding. Since radial flow is more representative of real field conditions, results obtained from radial discs should be more accurate as lab data for field implementation.

Briefly summarized, at low shear rates where amplitude of the elastic component is negligible, flow is controlled by shear forces. In contrast, above a critical shear rate, flow will be extensional and governed by elastic forces. Therefore, response of polymer solutions to imposed stress may be expressed as the sum of shear and elastic components:

$$\Delta P = \Delta P_{shear} + \Delta P_{elastic} \quad (26)$$

$$\mu = \mu_{shear} + \mu_{elastic} \quad (27)$$

Viscosity of polymer solutions under shear flow can be described by empirical equations such as power-law and Carreau model. To describe viscosity under elongational flow, several models have been suggested, and some of them are summarized in Table *2*.

2.3 Injectivity

Polymer injectivity is a crucial factor governing economics of polymer flooding projects and its accurate estimation is a prerequisite in terms of optimizing upper limit injection rate [79]. Injection well pressure may increase due to one of the following causes: (1) oil bank formation, (2) in-situ polymer viscosity (especially shear thickening due to viscoelasticity) and (3) different types of retention, which cause permeability reduction.

Highest pressure drops observed during polymer flooding is located in vicinity of injection wellbore due to dramatic variation in flow rate. Therefore, it is important to include non-Newtonian effects of polymer solutions to accurately predict polymer injectivity. Although both HPAM and Xanthan demonstrate shear thinning behavior at low to moderate shear rates, HPAM exhibit shear thickening above a critical flow rate due to its inherent viscoelastic nature. For field applications, injection rate at vicinity of injection well may easily exceed onset of extensional viscosity and injectivity will then dramatically decrease. In contrast to HPAM, Xanthan shows exclusively shear thinning behavior and will attain its highest value of injectivity in near wellbore region.

Injectivity investigation at the lab scale is required before implementing field applications and effects of polymer solution properties, in-situ rheology, temperature, PH, level of retention and nature of porous media should be accurately measured [76-78]. Furthermore, if screening criteria for polymer type is disregarded, polymer entrapment in narrow pore throats can have a significant effect on its injection rate. Salinity of solutions may also affect solubility of polymer, resulting in filter cake formation near injection wells or precipitate of polymer molecules in reservoir. Inaccurate measurement of in-situ rheology and especially onset of extensional viscosity may lead to either an underestimation or overestimation of injectivity. In some polymer flooding projects, measured injectivity may differ significantly from the simulation or analytical forecast. These unexpected injectivities may be due to occurrence of mechanical degradation [79-81], induced fractures [82-85] or even inaccurate analytical models for calculating in-situ rheology and prediction of extensional viscosity.

3. Radial in-situ rheology

Injectivity (I) may be defined as the ratio of volumetric injection rate, Q, to the pressure drop, ΔP, associated with polymer propagation between injection well and producer (Seright, [1]:

$$I = \frac{Q}{\Delta P} \tag{28}$$

As previously mentioned, formation fracture pressure may constrain the value of volumetric injection rate. Due to its significant effect on projects economics, accurate determination of differential pressure, and hence injectivity, at a given injection rate, is essential. To achieve this, all factors affecting differential pressure during polymer flooding must be quantified. Darcy's law for radial flow may be expressed in terms of differential pressure as follows:

$$\Delta P = \frac{\mu_{app} Q}{2\pi h k_{e,i}} ln \frac{r_e}{r_w} \quad (29)$$

Where μ_{app} is apparent viscosity, h is disc thickness, $k_{e,i}$ is effective permeability to polymer solution, r_e is disc radius and r_w is injection well radius.

In this paper, the ratio of resistance factor (RF) to residual resistance factor (RRF) is used to represent apparent viscosity of polymer solutions propagating through porous media, thus isolating its viscous behavior.

$$\mu_{app} = \frac{RF}{RRF} \quad (30)$$

Where resistance factor (RF) represents pressure increase of polymer relative to brine and residual resistance factor (RRF) is defined as ratio of pressure before and after polymer injection (i.e. pressure caused by irreversible permeability reduction induced by retention mechanisms).

Due to its inherent viscoelastic behavior in porous media, synthetic polymers (e.g. HPAM) will exhibit shear dependent apparent viscosity. Although common consensus on shear thickening as a phenomenon is highly accepted, its viscosifying magnitude is still an ongoing topic of debate in scientific communities.

Accurate polymer rheology estimation is a prerequisite for reasonable injectivity estimates due to the proportionality between apparent viscosity and differential pressure. In linear core floods where steady state pressure conditions governs, polymer flux will remain constant from inlet to outlet, rendering rheology estimation a straightforward task. However, in radial flow, polymer flux is gradually reduced as it propagates from injection well to producer, therefore attaining a range of viscosities rather than one specific value. Since the degree of mechanical degradation generally increase with injection rate, discrepancies in polymer rheology obtained from different injection rates may transpire. Instead of possessing one definite rheology, polymers propagating through radial discs will exhibit both shear dependent and history dependent viscosity behavior, thus increasing the complexity of rheology estimation in radial compared to linear models. To date, no correction factor has been suggested to account for this dual nature phenomenon. Even when mechanical degradation is excluded, i.e. when injected and effluent viscosities are approximately equal, this dual nature phenomenon persists, and is suggested to

be attributed to non-equilibrium pressure conditions experienced in radial flow and inherent history dependent nature of polymer molecules.

In addition, synthetic polymers are susceptible to mechanical degradation at high flux, typically in the near wellbore region, which will impart an irreversible viscosity reduction due to polymer molecule fragmentation. Mechanical degradation induces a pressure drop that improves injectivity. However, since it disrupts the carefully selected viscous properties of the polymer solutions by a non-reversible viscosity decrease, mechanical degradation is not a sought after phenomenon in polymer flooding. A remediation measure to reduce mechanical degradation is to pre-shear the polymer before injection. Preshearing will remove the high molecular part of the molecular weight distribution, which is believed to be most susceptible to mechanical degradation (Glasbergen, et al. [6]). Mechanical degradation may also be minimized by shifting to a lower molecular weight polymer. However, this would require higher amounts of polymer to obtain the same concentration, thus potentially influencing polymer project economics.

As mentioned, in radial geometry, high flux causing mechanical degradation occur principally in the near wellbore region, as opposed to linear geometry where this high flux persist throughout the entire propagation distance. Therefore, the time polymer is exposed to high shear is short in radial transient flow pattern, as opposed to that of a steady-state linear core flood, Skauge, et al., [33]. Based on this time-differing condition between linear and radial flow, it was suggested by Skauge, et al. that polymer is degraded to a less extent in radial compared to linear flood when injected at the same volumetric flow rate.

In summary, there are two principal factors governing injectivity during polymer flooding in linear geometry: (1) viscoelasticity of polymer that induces large injection pressures mainly due to shear thickening behavior at high flux and (2) mechanical degradation in near well-bore region, which causes an entrance pressure drop (Seright, [1]). In radial discs, two additional factors should be included: (3) non-equilibrium pressure conditions due to kinetic effects and (4) memory-effect of polymer molecules in non-constant velocity fields.

4. Materials and methods

Rock: Bentheimer outcrop rock (porosity of ~23 %, permeability of about 2.6 Darcy). Based on XRD measurements, Bentheimer consists of predominantly quartz (90.6 %) and with some feldspar (4.6 %), mica (3.2 %) and siderite (1.0 %) present.

Polymer: Flopaam 3630S, 30% hydrolyzed, MW = 18 million Dalton. 800 and 2000ppm (semi-dilute regime).

Brine: Relatively low salinity with a low content of divalent ions. Brine composition by ions is given in Table 5.

Linear core floods: Core data are summarized in Table 6. All experiments were performed at room temperature and pressure.

Radial core floods: Bentheimer discs were prepared by coating with epoxy resin, vacuuming and saturating with brine. One disc was then drained with a heavy oil and aged for 3 weeks at 50 C to a non-water-wet state. The heavy oil was then exchanged with a flooding oil of 210 cP. Both experiments were performed at room temperature and pressure. Core data are given in Table 7. The pressure ports were located in the injection and production wells and at radii 0.5, 1.0, 1.5, 2.0, 3.0, 4.0 and 5.0 cm for the disc without oil and at radii 1.1, 2.0 and 5.0 cm for the disc containing oil.

Simulation: Experimental set up enabled detailed monitoring of pressure by internal pressure ports located at various distance from injection well. Differential pressure as function of radial distance were history matched using STARS simulator, developed by Computer Modeling Group (CMG). The simulation model encompass a radial grid with 360 sectors, each consisting of 150 grid block cells in radial direction, where grid block cell size is 1 mm. Porous media permeability (tuning parameter) was obtained by history matching water floods prior to polymer flooding. Local permeability variation improved history match compared to analytical solution (Darcy's law for radial flow). Permeability field obtained from water floods were used in subsequent polymer floods to isolate effect of polymer apparent viscosity on differential pressure. In polymer floods, as permeability obtained from precursory water flood was held constant, apparent viscosity as function of velocity could be quantitatively investigated and was used as tuning parameter to history match differential pressure. STARS simulation tool can include both shear thinning and thickening behavior of viscoelastic fluids.

Due to the inherent grid averaging calculation method of simulation tool, velocity in first grid block after injection well was below its analytical value. Because of rapid velocity decrease with distance in radial models, this phenomenon was addressed by decreasing injection well radius, thus effectively parallel shifting position of first grid block towards injection well until correct velocity was attained. This was a necessary step since tuning parameter is apparent viscosity as function of velocity.

5. Polymer In-situ rheology in linear cores

Four Bentheimer outcrop cores were used to study polymer in-situ rheology in linear systems. Petro-physical properties of core samples as well as properties of polymer solutions are given in Table 6. Two experiments were carried out to examine the effect of polymer concentration on in-situ rheology of the polymer solution. Partially hydrolyzed polymer 3630s with molecular weight of about 18 MDa with concentration of 500 ppm and 1500 ppm was injected into the cores and in-situ rheology of the polymer solution was measured. The results are presented in Table 6 and Figure 4. Bulk viscosity of 1500 ppm 3630s is about 34 cP which is about 5 times that of 500 ppm 3630s. Comparing in-situ rheology of 500 ppm and 1500 ppm HPAM 3630s shows that onset and degree of shear thickening behavior are fairly similar for both concentrations. This is in line with observations by Skauge et al. [8] and Clarke et al. [59] that onset of extensional viscosity is independent of polymer concentration and only depends on polymer molecular weight. Table 6 and Figure 4 show that magnitude of resistance factor (RF) and residual resistance factor (RRF) are about 4 and 3 times higher for 1500 ppm compared to

500 ppm, respectively. This implies that polymer injectivity is a function of polymer concentration, and better injectivity is achieved with lower polymer concentrations.

A series of experiments were also performed to study the effect of presence of residual oil on polymer in-situ rheology. In these experiments, Bentheimer cores at residual oil saturation of about 22 percent and different initial wettability states were flooded with polymer and the in-situ rheology behavior was compared to that of single phase polymer injection in absence of residual oil. The results are presented and compared in Figure 5. As this figure shows the onset of shear thickening is not affected by presence of residual oil or wettability state of the cores. However, the slope of shear thickening and magnitude of resistance factor is significantly affected by oil presence in the cores. That is, although onset of shear thickening is independent of oil presence in porous media and its wettability condition, but the results show that the degree of shear thickening is lower when oil is present in the porous media.

It is important to note that lower resistance factor in presence of oil is achieved while porous media is partially occupied by residual oil, and therefore unlike the single phase system which the pore volume (assuming no inaccessible pore volume) is available for polymer flow, only PV*(1-Sor) is available for polymer flow in two phase system. This will influence and reduce permeability and therefore even higher resistance factor is expected in oil presence. However results do not show such an effect and lower resistance factor and better polymer injectivity is observed with oil presence in porous media which supports the significance of oil effect on better polymer injectivity.

Polymer injection in cores with residual oil results in lower resistance factor which means better polymer injectivity. Furthermore resistance factor in the aged core with non-water wet state is lower than resistance factor in water wet core. The lower resistance factor in presence of oil could be attributed to lower adsorption/retention of polymer molecules on rock surface Broseta et al. [10]. Rock surface in presence of oil film and especially in less water wet conditions is partially covered by polar components of crude oil during flooding. Therefore in comparison to single phase systems, rock surface has less adsorption sites on rock surface to adsorb polymer molecules. The analysis of reduced apparent viscosity in presence of oil, assumes that end-point water relative permeability remains constant for polymer as for water. The RRF measured with brine after the polymer injection is assumed constant for all rate variation of polymer flow. Under these assumptions lower resistance factor and better polymer injectivity is expected.

6. Polymer in-situ rheology in radial flow

Two radial flow experiments were performed on circular Bentheimer sandstone discs of 1.6 and 2.6 D permeability with 30 cm diameter and 2.2 cm thickness, see Table 7. The first experiment was performed on a disc that was drained with a crude oil and aged to non-water-wet conditions. The second experiment was performed in absence of oil on a water-wet disc. For the first experiment, the disc was flooded extensively with brine to reach residual oil saturation, Sorw = 0.22. Bump rates were applied to avoid oil mobilization by viscous forces during the subsequent polymer flood. The polymer flood was performed by first saturating the disc with

polymer at a low rate to avoid mechanical degradation due to shearing. Thereafter, rate variations were performed to determine in-situ rheology of the polymer. Brine flush was performed between concentration slugs to remove non-adsorbed polymer.

Concentrations of 800 and 2000 ppm were chosen to represent lower and upper boundaries of semi-dilute region. The second experiment included the same steps, except for water flooding to Sorw. In this case, water flood was performed to obtain a pressure reference for the subsequent polymer flood. No oil production was detected during polymer floods.

Differential pressure was measured by internal pressure ports located at different radii from the injection well. The 800-ppm HPAM solution was injected in presence of residual oil at flow rates of 2.2 and 2.8 mL/min, and in absence of residual oil at 2.0 and 4.0 mL/min. Differential pressure decay as a function of radial distance from injector is shown in Figure 6. The pressure transition zone from semi-steady state to steady state is extended compared to the case without oil. Most notable is the difference in pressure in the injection well. While differential pressures measured from internal pressure ports are higher for the two-phase system (as expected), well injection pressure is significantly lower in the presence of residual oil. Taking the pressure ratio of pressure ports at ~1 cm from injection well as a reference, injection pressure should have been 5-6 times higher for the disc with oil, compared to the one without. Instead, the injection pressure is 25 % lower. There may be several reasons for this observation. One reason may be that presence of oil reduces effective pore volume, thereby leading to higher flow velocities for the polymer in the near-well region. This would subsequently lead to higher effective shear forces on the polymer, leading to mechanical degradation. If mechanical degradation occurs, it only has a minor effect on the shear viscosity. The shear viscosity is 15.1 mPas for the effluent sample taken at 2.0 ml/min, while it was 16.0 mPas for the injected solution (measured at 22 C, 10 1/s). However, as discussed in chapter 2.2, it is the extensional viscosity that is the determining factor for high pressures in near-well region. Changes in extensional viscosity are intrinsically hard to measure and were not performed here. It is still possible that increase in shear forces for the case with residual oil lead to a reduction in extensional viscosity and not for the case without oil where effective pore volume was larger. The two other reasons are related to the wetting state of the porous media. If the oil is located in smaller pores, polymer flow is diverted to larger pores where it flows at higher velocities (higher flux). Since the velocity increase takes place in larger pores, only minor degradation would be expected. A third reason may be that porous media is fractionally oil-wet and that the oil “coating” on the rock surface reduces effective shear enforced by porous media on polymer. It is not possible to differentiate between the three phenomena based on the pressure data alone.

To evaluate influence of polymer concentration on in-situ rheology, 2000 ppm HPAM was injected in both discs. The differential pressures are shown in Figure 8. In this case, the injection rates were Q = 2.0 and 5.0 ml/min for the disc with no oil, and Q = 1.4 and 1.6 ml/min for the disc with oil. These data show the same trend as for the 800 ppm injection: strong reduction in injection well pressure in the presence of residual oil and extension of the transition zone.

Each of the polymer floods were history matched using STARS (CMG). The measured differential pressures as function of distance from injection well were used as history match

parameters, while polymer apparent viscosity was used as tuning variable. History matches and polymer rheology from both experiments for 800-ppm HPAM floods are shown in figure 6 and 7, respectively. Evident from figure 7, polymer rheology is significantly influenced by presence of residual oil. In terms of absolute values, apparent viscosity is between a factor of 5 to 10 higher in absence compared to presence of residual oil. Furthermore, onset of shear thickening shifts to lower velocities in presence of residual oil. This occurrence is suggested to result from reduced propagation cross section caused by the residual oil saturation. When flow channels in porous media become narrower, extensional flow regime will be reached at lower flux and HPAM will exhibit viscoelastic behavior at an earlier stage, thus onset of shear thickening commences at lower flux. Isolated effect of shifting onset of shear thickening to lower flux may be malicious for injectivity. However, since shear thickening seems to be much more extensive in absence of residual oil, rheology shows that overall injectivity is significantly improved in presence of residual oil.

History matches and polymer rheology in presence and absence of residual oil for 2000-ppm floods are shown in figure 8 and 9, respectively. In accordance with the 800-ppm solution, polymer viscosity was significantly higher in absence compared to presence of residual oil, and ranged between a factor of 6 to 16 in their joint velocity interval. In addition, the 2000-ppm solution also showed a decrease in onset of shear thickening in presence of residual oil, consistent with the lower concentration solution investigated. Similar to the 800-ppm solution, shear thickening is observed to be much more extensive in absence of residual oil, thus improved injectivity in presence of residual oil is further corroborated.

7. Conclusions

A theoretic review of polymer flow in porous medium has been presented. The available EOR analytical models we have evaluated, have limitations in accurately describing flow of polymer at high shear rates e.g., near injector, and this leads to underestimating or overestimating of polymer injectivity.

Experimental results presented expands our in-sight into polymer flow in porous medium. Shear thinning behavior may be present in core floods while rheology is predominant in rheometer measurements. Linear polymer flow experiments are dominated by shear thickening which are not measured in standard rheometers. The extensional viscosity, that is the main cause of the shear thickening behavior, occurs at flow velocities strongly influenced by the porous media.

Linear core floods are commonly used for evaluating polymer in-situ rheology and injectivity, but suffer from steady state conditions over the core as opposed to the well injection situation where both pressure and shear forces are non-linear gradients.

In the linear core floods, the onset of shear thickening is independent of polymer concentration, when polymer type, brine composition and porous media are held constant. It is also independent of the presence of oil and wettability for the three cases evaluated here.

Radial flow injections show more complex in-situ rheology. The in-situ rheology shows a much higher degree of shear thickening in the presence of oil. This may be due to restrictions in the pore space available. In the absence of oil, high concentration polymer (2000 ppm) showed shear thinning behavior. The onset of shear thickening was shifted to higher flow velocities. There is a need for further development of the numerical models that incorporates memory effect and possible kinetics effects for high polymer flow rates in the near-well region.

Both linear and radial experiments confirm lower apparent viscosity when oil is present in the porous medium. This conclusion is based on the assumption that brine end-point relative permeability is unchanged for polymer injection compared to two-phase flow by water injection. No extra oil was produced during polymer injection and this support the lowering of in-situ polymer viscosity in presence of oil.

Acknowledgments: The authors gratefully acknowledge support from the Norwegian Research Council, Petromaks 2 program. Badar Al Shakry acknowledge support from, PDO, Petroleum Development Oman. Arne Skauge acknowledge support from Energi Simulations, Canada as an EOR chair at University of Bergen.

Author Contributions: A. Skauge, B.S. Shiran, and T. Skauge were responsible for the experimental program and simulation study. N. Zamani structured the theoretic contribution, while B. AlShakry and J. Jacobsen are PhD students working on polymer injectivity, both from experimental study and simulation of experiments. All authors contributed in writing the paper.

Conflicts of Interest: The authors declare no conflicts of interest.

Nomenclature

A	Cross section area	α	Correction factor
C	Power law constant	β	Constant, equation 10
C_p	Polymer concentration	ω	Angular velocity
D_p	Grain size diameter	$\dot{\varepsilon}$	Stretch rate
De	Deborah number	ΔP	Pressure drop
h	Disc thickness	$\dot{\gamma}$	Shear rate
H	Constant, equation 11	$\tau_{1/2}$	Ellis model parameter
k	Constant, equation 18.	$\dot{\gamma}_{eff}$	Effective shear rate
K_{ei}	Effective permeability to polymer	$\dot{\gamma}_{app}$	Apparent shear rate
K	Permeability	$\dot{\gamma}_c$	Critical shear rate
L	Length of model	λ	Polymer relaxation time
M_w	Polymer molecular weight	λ_z	Zimm relaxation time
N_1	Normal stress difference	μ	Viscosity

n	Ellis, Carreau or power law constant	μ_{app}	Apparent viscosity
P	Pressure	μ_{eff}	Effective viscosity
Q	Flow rate	μ_0	Upper Newtonian plateau
R	Radius	μ_s	Solvent viscosity
r_e	Disc radius	μ_{sh}	Shear rate viscosity
r_w	Injection well radius	μ_e	Elongational viscosity
RF	Resistance factor	μ_∞	Lower Newtonian plateau
RRF	Residual resistance factor	ϕ	Porosity
R_{eq}	Equivalent radius obtained from Blake-Kozeny model	ψ	Tortuosity
S_w	Water saturation	θ_f	Characteristic relaxation time of fluid
T	Temperature	θ_p	Characteristic time of porous media
Tr	Trouton ratio		
u	Darcy velocity		
Wi	Weissenberg number		
I	Injectivity		

References

1. Seright, R.S. The Effects of Mechanical Degradation and Viscoelastic Behavior on Injectivity of Polyacrylamide Solutions. *Society of Petroleum Engineers Journal* **1983**, *23*, 475-485. SPE-9297-PA. https://doi.org/10.2118/9297-PA.

2. Shuler, P.J.; Kuehne, D.L.; Uhl, J.T.; Walkup Jr, G.W. Improving Polymer Injectivity at West Coyote Field, California. *Society of Petroleum Engineers Reservoir Engineering* **1987**, *2,* 271-280. SPE-13603-PA. https://doi.org/10.2118/13603-PA.

3. Southwick, J.G.; Manke, C.W. Molecular Degradation, Injectivity, and Elastic Properties of Polymer Solutions. *Society of Petroleum Engineers Reservoir Engineering* **1988**, *3*, 1193-1201. SPE-15652-PA. https://doi.org/10.2118/15652-PA.

4. Yerramilli, S.S.; Zitha, P.L.J.; Yerramilli, R.C. Novel Insight into Polymer Injectivity for Polymer Flooding. Presented at the *SPE European Formation Damage Conference and Exhibition*, Noordwijk, Holland, **2013**. 5-7 June. SPE-165195-MS. https://doi.org/10.2118/165195-MS.

5. Lotfollahi, M.; Farajzadeh, R.; Delshad, M.; Al-Abri, K.; Wassing, B.M.; Mjeni, R.; Awan, K.; Bedrikovetsky, P. Mechanistic Simulation of Polymer Injectivity in Field Tests. Presented

at the *SPE Enhanced Oil Recovery Conference*, Kuala Lumpur, Malaysia, **2015**. 11-13 August. SPE-174665-MS. https://doi.org/10.2118/174665-MS.

6. Glasbergen, G.; Wever, D.; Keijzer, E.; Farajzadeh, R. Injectivity Loss in Polymer Floods: Causes, Preventions and Mitigations. Presented at the *SPE Kuwait Oil & Gas Show and Conference*, Mishref, Kuwait, **2015**. 11-14 October. SPE-175383-MS. https://doi.org/10.2118/175383-MS.

7. Al-Shakry, B.; Shiran, B.S.; Skauge, T.; Skauge, A. Enhanced Oil Recovery by Polymer Flooding: Optimizing Polymer Injectivity. Prepared for presentation at the *SPE Kingdom of Saudi Arabia Technical Symposium and Exhibition*, Dammam, Saudi Arabia, **2018**. 23-26 April. SPE-899-MS.

8. Skauge, T.; Kvilhaug O.A.; Skauge, A. Influence of Polymer Structural Conformation and Phase Behaviour on In-situ Viscosity. Presented at the *18th European Symposium on Improved Oil Recovery*, Dresden, Germany, **2015**. 14-16 April. https://doi.org/10.3997/2214-4609.201412154.

9. Hughes, D.S.; Teeuw, D.; Cottrell, C.W.; Tollas, J.M. Appraisal of the Use of Polymer Injection To Suppress Aquifer Influx and To Improve Volumetric Sweep in a Viscous Oil Reservoir. *Society of Petroleum Engineers* **1990**, *5*, 33-40. https://doi.org/10.2118/17400-PA.

10. Broseta, D.; Medjahed, F.; Lecourtier, J.; Robin, M. Polymer Adsorption/Retention in Porous Media: Effects of Core Wettability on Residual Oil. *Society of Petroleum Engineers* **1995**, *3*, 103-112. https://doi.org/10.2118/24149-PA.

11. Savins, J.G. Non-Newtonian Flow through Porous Media. *Industrial and Engineering Chemistry* **1969**, *61*, 18-47. https://doi.org/10.1021/Ie50718a005.

12. Sadowski, T.J. Non-Newtonian Flow through Porous Media. II. Experimental. *Journal of Rheology* **1965**, *9*, 251-271. https://doi.org/10.1122/1.549023.

13. Sochi, T. Non-Newtonian flow in porous media. *Polymer* **2010**, *51*, 5007-5023. https://doi.org/10.1016/j.polymer.2010.07.047.

14. Sadowski, T.J; Bird, R.B. Non-Newtonian Flow through Porous Media. I. *Journal of Rheology* **1965**, *9*, 243-250. https://doi.org/10.1122/1.549000.

15. Teeuw, D; Hesselink, F.T. Power-Law Flow And Hydrodynamic Behaviour Of Biopolymer Solutions In Porous Media. Presented at the *SPE Fifth International Symposium on Oilfield and Geothermal Chemistry*, Stanford, California, **1980**, 28-30 May. SPE-8982-MS. https://doi.org/10.2118/8982-MS.

16. Cannella, W.J.; Huh, C.; Seright, R.S. Prediction of Xanthan Rheology in Porous Media. Prepared for presentation at the *63rd Annual Technical Conference and Exhibition of the Society of Petroleum Engineers*, Houston, Texas, **1988**. 2-5 October. SPE-18089-MS. https://doi.org/10.2118/18089-MS.

17. Fletcher, A. J. P.; Flew, S.R.G.; Lamb, S.P.; Lund, T.; Bjornestad, E.; Stavland, A.; Gjovikli, N.B. Measurements of Polysaccharide Polymer Properties in Porous Media. Prepared for presentation at the *SPE International Symposium on Oilfield Chemistry*, Anaheim, California, **1991**. 20-22 February. SPE-21018-MS. https://doi.org/10.2118/21018-MS.

18. Lopez, X.; Valvatne, P.H.; Blunt, M.J. Predictive network modeling of single-phase non-Newtonian flow in porous media. *Journal of Colloid and Interface Science* **2003**, *264*, 256-265. https://doi.org/10.1016/S0021-9797(03)00310-2.

19. Pearson, J.R.A.; Tardy, P.M.J. Models for flow of non-Newtonian and complex fluids through porous media. *Journal of Non-Newtonian Fluid Mechanics* **2002**, *102*, 447-473. https://doi.org/10.1016/S0377-0257(01)00191-4.

20. Sorbie, K.S. *Polymer-Improved Oil Recovery*. Blackie and Son Ltd.: Glasgow, Scotland, 1991.

21. Lake, L.W. *Enhanced oil recovery*. Prentice Hall: New Jersey, USA, 1989.

22. Willhite, G.P.; J.T. Uhl, *Correlation of the Flow of Flocon 4800 Biopolymer with Polymer Concentration and Rock Properties in Berea Sandstone*, in *Water-Soluble Polymers for Petroleum Recovery*. Springer Publishing: Manhattan, New York, New York, 1988.

23. Bird, R.B.; Stewart, W.E.; Lightfoot, E.N. *Transport phenomena*. John Wiley and Sons, Inc.: New York, New York, 1960.

24. Christopher, R.H.; Middleman, S. Power-Law Flow through a Packed Tube. *Industrial & Engineering Chemistry Fundamentals* **1965**, *4*, 422-426. https://doi.org/10.1021/i160016a011.

25. Hirasaki, G.J; Pope, G.A. Analysis of Factors Influencing Mobility and Adsorption in the Flow of Polymer Solution Through Porous Media. *Society of Petroleum Engineers Journal* **1974**, *14*, 337-346. SPE-4026-PA. https://doi.org/10.2118/4026-PA.

26. Duda, J.L.; Hong, S-A.; Klaus, E.E. Flow of Polymer-Solutions in Porous-Media - Inadequacy of the Capillary Model. *Industrial & Engineering Chemistry Fundamentals* **1983**, *22*, 299-305. https://doi.org/10.1021/I100011a005.

27. Gogarty, W.B. Rheological Properties of Pseudoplastic Fluids in Porous Media. *Society of Petroleum Engineers Journal* **1967**, *7*, 149-160. SPE-1566-A. https://doi.org/10.2118/1566-A.

28. Zamani, N.; Bondino, I.; Kaufmann, R.; Skauge, A. Computation of polymer in-situ rheology using direct numerical simulation. *Journal of Petroleum Science and Engineering* **2017**, *159*, 92-102. https://doi.org/10.1016/j.petrol.2017.09.011.

29. Balhoff, M.T.; Thompson, K.E. A macroscopic model for shear-thinning flow in packed beds based on network modeling. *Chemical Engineering Science* **2006**, *61*, 698-719. http://doi.org/10.1016/j.ces.2005.04.030.

30. Perrin, C.L.; Tardy, P.M.J.; Sorbie, K.S.; Crawshaw, J.C. Experimental and modeling study of Newtonian and non-Newtonian fluid flow in pore network micromodels. *Journal of Colloid and Interface Science* **2006**, *295*, 542-550. http://doi.org/10.1016/j.jcis.2005.09.012.

31. Sochi, T.; Blunt, M.J. Pore-scale network modeling of Ellis and Herschel–Bulkley fluids. *Journal of Petroleum Science and Engineering* **2008**, *60*, 105-124. http://doi.org/10.1016/j.petrol.2007.05.009.

32. Hejri, S.; Willhite, G.P.; Green, D.W. Development of Correlations To Predict Biopolymer Mobility in Porous Media. *SPE Reservoir* Engineering **1991**, *6*, 91-98. SPE-17396-PA. https://doi.org/10.2118/17396-PA.

33. Skauge, T.; Skauge, A.; Salmo, I.C.; Ormehaug, P.A.; Al-Azri, N.; Wassing, L.M.; Glasbergen, G.; Van Wunnik, J.N.; Masalmeh, S.K. Radial and Linear Polymer Flow - Influence on Injectivity. Prepared for presentation at the *SPE Improved Oil Recovery Conference*, Tulsa, Oklahoma, **2016**. 11-13 April. SPE-179694-MS. https://doi.org/10.2118/179694-MS.

34. Faber, T.E. *Fluid Dynamics for Physicists*. Cambridge University Press: Cambridge, United Kingdom, 1995.

35. Brown, E.; Jaeger, H.M. The role of dilation and confining stresses in shear thickening of dense suspensions. *Journal of Rheology* **2012**, *56*, 875-923. https://doi.org/10.1122/1.4709423.

36. Choplin, L.; Sabatie, J. Threshold-Type Shear-Thickening in Polymeric Solutions. *Rheologica Acta* **1986**, *25*, 570-579. https://doi.org/10.1007/Bf01358165.

37. Indei, T.; Koga, T.; Tanaka, F. Theory of shear-thickening in transient networks of associating polymer. *Macromolecular Rapid Communications* **2005**, *26*, 701-706. https://doi.org/10.1002/marc.200500009.

38. Odell, J.A.; Müller, A.J.; Keller, A. Non-Newtonian behaviour of hydrolysed polyacrylamide in strong elongational flows: a transient network approach. *Polymer* **1988**, *29*, 1179-1190. http://doi.org/10.1016/0032-3861(88)90042-0.

39. Degennes, P.G. Coil-Stretch Transition of Dilute Flexible Polymers under Ultrahigh Velocity-Gradients. *Journal of Chemical Physics* **1974**, *60*, 5030-5042. https://doi.org/10.1063/1.1681018.

40. Trouton, F.T. On the coefficient of viscous traction and its relation to that of viscosity. *The Royal Society* **1906**, *77*, 426-440. https://doi.org/10.1098/rspa.1906.0038.

41. Kishbaugh, A.J.; McHugh, A.J. A rheo-optical study of shear-thickening and structure formation in polymer solutions. Part I: Experimental. *Rheologica Acta* **1993**, *32*, 9-24. https://doi.org/10.1007/bf00396673.

42. Edwards, B.J.; Keffer, D.I.; Reneau, C.W. An examination of the shear-thickening behavior of high molecular weight polymers dissolved in low-viscosity newtonian solvents. *Journal of Applied Polymer Science* **2002**, *85*, 1714-1735. https://doi.org/10.1002/app.10807.

43. Hatzignatiou, D.G.; Moradi, H.; Stavland, A. Experimental Investigation of Polymer Flow through Water- and Oil-Wet Berea Sandstone Core Samples. Prepared for presentation at the *EAGE Annual Conference & Exhibition incorporationg SPE* Europec, London, United Kingdom, **2013**. 10-13 June. SPE-164844-MS. https://doi.org/10.2118/164844-MS.

44. McKinley, G.H.; Sridhar, T. Filament-stretching rheometry of complex fluids. *Annual Review of Fluid Mechanics* **2002**, *34*, 375-415. https://doi.org/10.1146/annurev.fluid.34.083001.125207.

45. Fuller, G.G.; Cathey, C.A.; Hubbard, B.; Zebrowski, B.E. Extensional Viscosity Measurements for Low-Viscosity Fluids. *Journal of Rheology* **1987**, *31*, 235-249. https://doi.org/10.1122/1.549923.

46. Meadows, J.; Williams, P.A.; Kennedy, J.C. Comparison of the Extensional and Shear Viscosity Characteristics of Aqueous Hydroxyethylcellulose Solutions. *Macromolecules* **1995**,

28, 2683-2692. https://doi.org/10.1021/Ma00112a013.

47. Pope, D.P.; Keller, A. Alignment of Macromolecules in Solution by Elongational Flow - Study of Effect of Pure Shear in a 4 Roll Mill. *Colloid and Polymer Science* **1977**, *255*, 633-643. https://doi.org/10.1007/Bf01550050.

48. Binding, D.M.; Jones, D.M.; Walters, K. The Shear and Extensional Flow Properties of M1. *Journal of Non-Newtonian Fluid Mechanics* **1990**, *35*, 121-135. https://doi.org/10.1016/0377-0257(90)85042-W.

49. Anna, S.L.; McKinley, G.H.; Nguyen, D.A.; Sridhar, T.; Muller, S.J.; Huang, J.; James, J.F. An interlaboratory comparison of measurements from filament-stretching rheometers using common test fluids. *Journal of Rheology* **2001**, *45*, 83-114. https://doi.org/10.1122/1.1332388.

50. Shipman, R.W.G.; Denn, M.M.; Keunings, R. Mechanics of the Falling Plate Extensional Rheometer. *Journal of Non-Newtonian Fluid Mechanics* **1991**, *40*, 281-288. https://doi.org/10.1016/0377-0257(91)87013-N.

51. Sridhar, T.; Tirtaatmadja, V.; Nguyen, D.A.; Gupta, R.K. Measurement of Extensional Viscosity of Polymer-Solutions. *Journal of Non-Newtonian Fluid Mechanics* **1991**, *40*, 271-280. https://doi.org/10.1016/0377-0257(91)87012-M.

52. Tirtaatmadja, V.; Sridhar, T. A Filament Stretching Device for Measurement of Extensional Viscosity. *Journal of Rheology* **1993**, *37*, 1081-1102. https://doi.org/10.1122/1.550372.

53. James, D.F.; Chandler, G.M.; Armour, S.J. A Converging Channel Rheometer for the Measurement of Extensional Viscosity. *Journal of Non-Newtonian Fluid Mechanics* **1990**, *35*, 421-443. https://doi.org/10.1016/0377-0257(90)85063-5.

54. Chauveteau, G. Moluecular interpretation of several different properties of flow of coiled polymer solutions through porous media in oil recovery conditions. Presented at the *56th Annual Fall Technical Conference and Exhibition of the society of Petroleum Engineers of AIME*, San Antonio, Texas, **1981**. 5-7 October. SPE-10060-MS. https://doi.org/10.2118/10060-MS.

55. Lewandowska, K. Comparative studies of rheological properties of polyacrylamide and partially hydrolyzed polyacrylamide solutions. *Journal of Applied Polymer Science* **2007**, *103*, 2235-2241. https://doi.org/10.1002/app.25247.

56. Briscoe, B.; Luckham, P.; Zhu, S.P. Pressure influences upon shear thickening of poly(acrylamide) solutions. *Rheologica Acta* **1999**, *38*, 224-234. https://doi.org/10.1007/s003970050172.

57. Dupuis, D.; Lewandowski, F.Y.; Steiert, P.; Wolff, C. Shear Thickening and Time-Dependent Phenomena - the Case of Polyacrylamide Solutions. *Journal of Non-Newtonian Fluid Mechanics* **1994**, *54*, 11-32. https://doi.org/10.1016/0377-0257(94)80013-8.

58. Jiang, B.; Keffer, D.J.; Edwards, B.J.; Allred, J.N. Modeling shear thickening in dilute polymer solutions: Temperature, concentration, and molecular weight dependencies. *Journal of Applied Polymer Science* **2003**, *90*, 2997-3011. https://doi.org/10.1002/App.12950.

59. Clarke, A.; Howe, A.M.; Mitchell, J.; Staniland, J.; Hawkes, L.A. How Viscoelastic-Polymer Flooding Enhances Displacement Efficiency. *Society of Petroleum Engineers Journal* **2016**, *21*, 675-687. SPE-174654-MS. https://doi.org/10.2118/174654-MS.

60. Aitkadi, A.; Carreau, P.J.; Chauveteau, G. Rheological Properties of Partially Hydrolyzed Polyacrylamide Solutions. *Journal of Rheology* **1987**, *31*, 537-561. https://doi.org/10.1122/1.549959.

61. Hu, Y.; Wang, S.Q.; Jamieson, A.M. Rheological and Rheooptical Studies of Shear-Thickening Polyacrylamide Solutions. *Macromolecules* **1995**, *28*, 1847-1853. https://doi.org/10.1021/Ma00110a019.

62. Cho, Y.H.; Dan, K.S.; Kim, B.C. Effects of dissolution temperature on the rheological properties of polyvinyl alchol solutions in dimethyl sulfoxide. *Korea-Australia Rheology Journal* **2008**, *20*, 73-77.

63. Zamani, N.; Bondino, I.; Kaufmann, R.; Skauge, A. Effect of porous media properties on the onset of polymer extensional viscosity. *Journal of Petroleum Science and Engineering* **2015**, *133*, 483-495. https://doi.org/10.1016/j.petrol.2015.06.025.

64. Gupta, R.K.; Sridhar, T. Viscoelastic Effects in Non-Newtonian Flows through Porous-Media. *Rheologica Acta* **1985**, *24*, 148-151. https://doi.org/10.1007/Bf01333242.

65. Smith, F.W. Behavior of Partially Hydrolyzed Polyacrylamide Solutions in Porous Media. *Journal of Petroleum Technology* **1970**, *22*, 148-156. https://doi.org/10.2118/2422-PA.

66. Kemblowski, Z.; Dziubinski, M. Resistance to Flow of Molten Polymers through Granular Beds. *Rheologica Acta* **1978**, *17*, 176-187. https://doi.org/10.1007/Bf01517709.

67. Wissler, E.H. Viscoelastic Effects in the Flow of Non-Newtonian Fluids through a Porous Medium. *Industrial & Engineering Chemistry Fundamentals* **1971**, *10*, 411-417. https://doi.org/10.1021/i160039a012.

68. Vossoughi, S.; Seyer, F.A. Pressure-Drop for Flow of Polymer-Solution in a Model Porous-Medium. *Canadian Journal of Chemical Engineering* **1974**, *52*, 666-669.

69. Marshall, R.J.; Metzner, A.B. Flow of Viscoelastic Fluids through Porous Media. *Industrial & Engineering Chemistry Fundamentals* **1967**, *6*, 393-400. https://doi.org/10.1021/I160023a012.

70. Durst, F.; Haas, R.; Interthal, W. Laminar and Turbulent Flows of Dilute Polymer-Solutions - a Physical Model. *Rheologica Acta* **1982**, *21*, 572-577. https://doi.org/10.1007/Bf01534350.

71. Heemskerk, J.; Rosmalen, R.; Janssen-van, R.; Holtslag, R.J.; Teeuw, D. Quantification of Viscoelastic Effects of Polyacrylamide Solutions. Presented at the *SPE/DOE Fourth Symposium on Enhanced Oil Recovery*, Tulsa, Oklahoma, **1984**. 15-18 April. https://doi.org/10.2118/12652-MS.

72. Metzner, A.B.; White, J.L.; Denn, M.M. Constitutive equations for viscoelastic fluids for short deformation periods and for rapidly changing flows: Significance of the deborah number. *AIChE Journal* **1966**, *12*, 863-866. https://doi.org/10.1002/aic.690120507.

73. Garrouch, A.A.; Gharbi, R.C. A Novel Model for Viscoelastic Fluid Flow in Porous Media. Prepared for presentation at the *2006 SPE Annual Technical Conference and Exhibition*, San Antonio, Texas, **2006**. 24-27 September. SPE-102015-MS. https://doi.org/10.2118/102015-MS.

74. Ranjbar, M.; Rupp, J.; Pusch, G.; Meyn, R. Quantification and Optimization of Viscoelastic Effects of Polymer Solutions for Enhanced Oil Recovery. Prepared for presentation at the

SPE/DOE Eight Symposium on Enhanced Oil Recovery, Tulsa, Oklahoma, **1992**. 22-24 April. https://doi.org/10.2118/24154-MS.

75. Kawale, D.; Marques, E.; Zitha, P.L.J.; Kreutzer, M.T.; Rossen, W.R.; Boukany, P.E. Elastic instabilities during the flow of hydrolyzed polyacrylamide solution in porous media: effect of pore-shape and salt. *Soft Matter* **2017**, *13*, 765-775. https://doi.org/10.1039/C6SM02199A.

76. Delshad, M.; Kim, D.H.; Magbagbeola, O.A.; Huh, C.; Pope, G.A.; Tarahhom, F. Mechanistic Interpretation and Utilization of Viscoelastic Behavior of Polymer Solutions for Improved Polymer-Flood Efficiency. Prepared for presentation at the *2008 SPE/DOE Improved Oil Recovery Symposium*, Tulsa, Oklahoma, **2008**. 19-23 April. SPE-113620-MS. https://doi.org/10.2118/113620-MS.

77. Kulawardana, E.U.; Koh, H.; Kim, D.H.; Liyanage, P.J.; Upamali, K.; Huh, C.; Weerasooriya, U.; Pope, G.A. Rheology and Transport of Improved EOR Polymers under Harsh Reservoir Conditions. Prepared for presentation at the *Eighteenth SPE Improved Oil Recovery Symposium*, Tulsa, Oklahoma, **2012**. 14-18 April. SPE-154294-MS. https://doi.org/10.2118/154294-MS.

78. Sharma, A.; Delshad, M.; Huh, C.; Pope, G.A. A Practical Method to Calculate Polymer Viscosity Accurately in Numerical Reservoir Simulators. Prepared for presentation at the *SPE Annual Technical Conference and Exhibition*, Colorado, Denver, USA, **2011**. 31 October - 2 November. SPE-147239-MS. https://doi.org/10.2118/147239-MS.

79. Seright, R.S.; Seheult, J.M.; Talashek, T. Injectivity Characteristics of EOR Polymers. *SPE Reservoir Evaluation & Engineering* **2009**, *12*, 783-792. https://doi.org/10.2118/115142-MS.

80. Manichand, R.N.; Moe Soe Let, K.P.; Gil, L.; Quillien, B.; Seright, R.S. Effective Propagation of HPAM Solutions Through the Tambaredjo Reservoir During a Polymer Flood. *SPE Production & Operations* **2013**, *28*, 358-368. https://doi.org/10.2118/164121-PA.

81. Zaitoun, A.; Makakou, P.; Blin, N.; Al-Maamari, R.S.; Al-Hashmi, A.-A.R.; Abdel-Goad, M.; Al-Sharji, H.H. Shear Stability of EOR Polymers. *SPE Journal* **2011**, *17*, 335-339. https://doi.org/10.2118/141113-MS.

82. Lee, K.; Huh, C.; Sharma, M.M. Impact of Fractures Growth on Well Injectivity and Reservoir Sweep during Waterflood and Chemical EOR Processes. Prepared for presentation at the *SPE Annual Technical Conference and* Exhibition, Denver, Colorado, USA, **2011**. 30 October - 2 November. SPE-146778-MS. https://doi.org/10.2118/146778-MS.

83. Suri, A.; Sharma, M.M.; Peters, E. Estimates of Fracture Lengths in an Injection Well by History Matching Bottomhole Pressures and Injection Profile. *SPE Reservoir Evaluation & Engineering* **2011**, *14*, 405 - 417. https://doi.org/10.2118/132524-PA.

84. Zechner, M.; Clemens, T.; Suri, A.; Sharma, M.M. Simulation of Polymer Injection under Fracturing Conditions - A Field Pilot in the Matzen Field, Austria. *SPE Reservoir Evaluation & Engineering* **2014**, *18*, 236-249. https://doi.org/10.2118/169043-MS.

85. van den Hoek, P.; Mahani, H.; Sorop, T.; Brooks, D.; Zwaan, M.; Sen, S.; Shuaili, K.; Saadi, F. Application of Injection Fall-Off Analysis in Polymer flooding. Prepared for presentation at the *74th EAGE Conference & Exhibition incorporating SPE EUROPEC* 2012, Copenhagen, Denmark, **2012**. 4-7 June. SPE-154376-MS. https:/doi.org/10.2118/154376-MS.

Preprints (www.preprints.org) | NOT PEER-REVIEWED | Posted: 1 June 2018 doi:10.20944/preprints201806.0015.v1

Peer-reviewed version available at Colloids Interfaces 2018, 2, 27; doi:10.3390/colloids2030027

Tables

Table 1. Summary of proposed models for correction factor (α)

Model	Equation for correction factor (α)	Description
Analytical solution	$4\left(\frac{3n+1}{4n}\right)^{\frac{n}{n-1}}$	*n* is the power index in power-law region
Hirasaki and Pope (1974)[46]	$\frac{12}{\sqrt{150}}\left(\frac{3n+1}{4n}\right)^{\frac{n}{n-1}}$	*n* is the power index in power-law region
Cannella et al. (1988)[42]	$\frac{\beta}{\sqrt{S_w}}\left(\frac{3n+1}{n}\right)^{\frac{n}{n-1}}$	*n* is the power index in power-law region, S_w is water saturation, β is a constant equal to 6.

Table 1: applied β values by different authors where ψ = 25/12

Model	B
Bird et al. (1960)	$\sqrt{2\psi}$
Christopher and Middleman (1965)	$\sqrt{\frac{2}{\psi}}$
Teeuw and Hesselink	$\sqrt{2}$

Table 3. Proposed equations for Deborah number calculation

Model	Equation	Description
Masuda et al. (1992)[59]	$N_{De} = \theta_f \, \dot{\gamma}_{eq}$ $\dot{\gamma}_{eq} = \frac{\dot{\gamma}_c \lvert u_w \rvert}{\sqrt{\bar{k}\, k_{rw} \phi S_w}}$	They used the inverse of the shear rate for θ_p. u_w is the Darcy velocity, k_{rw} is the water relative permeability, S_w is water saturation and $\dot{\gamma}_c$ is a constant equal to 3.97C and C is an empirical correlation factor to account for the difference between an equivalent capillary model and real porous media
Hirasaki and Pope (1974)[46] Haas and Durst(1981)[100] Heemskerk et al. (1984)[101]	$\frac{1}{\theta_p} = \dot{\varepsilon} = \frac{v}{d} = \frac{u_w}{(1-\phi S_w)\sqrt{150 K K_r/(\phi S_w)}}$	

Preprints (www.preprints.org) | NOT PEER-REVIEWED | Posted: 1 June 2018 doi:10.20944/preprints201806.0015.v1

Peer-reviewed version available at Colloids Interfaces 2018, 2, 27; doi:10.3390/colloids2030027

Table 2. Proposed models for calculation of elongational viscosity

Model	Equation	Description
Hirasaki and Pope (1974)[46]	$\mu_{el} = \frac{\mu_{sh}}{[1 - N_{De}]}$	
Masuda et al. (1992)[59]	$\mu_{elas} = \mu_{sh} C_c (N_{De})^{m_c}$	Where C_c and m_c are constant and relate to pore geometry
Delshad et al. (2008)[58]	$\mu_{el} = \mu_{max}[1 - \exp(-(\lambda_2 \tau_r \dot{\gamma})^{n_2 - 1})]$ $\tau_r = \tau_1 + \tau_0 C_p$ $\mu_{max} = \mu_w (AP_{11} + AP_{22} \ln C_p)$	τ_r is the characteristic relaxation time and can be calculated by dynamic frequency sweep test in the laboratory. Some empirical correlations are also proposed for dependency of different parameters on polymer concentration
Stavland et al. (2010)[104]	$\mu_{el} = (\lambda_2 \dot{\gamma})^m$ $\lambda_2 = \left\{ N_{De} \left(\frac{1 - \phi}{\phi} \right) \left(\frac{6\alpha \sqrt{\tau}}{\lambda_1} \right) \right\}^{-1}$	m is a non-zero tuning parameter which is known as the elongation exponent and depends on the molecular weight and demonstrates linear correlation with $[\mu]C_p$. α in the above formulation is considered as 2.5

Table 5. Brine ionic composition

Ion	**Concentration (ppm, w/w)**
Na	1741
K	28
Ca	26
Mg	17
SO_4	160
Cl	2687
TDS	4659
Ionic strength	0.082
Hardness	43

Preprints (www.preprints.org) | NOT PEER-REVIEWED | Posted: 1 June 2018 doi:10.20944/preprints201806.0015.v1

Peer-reviewed version available at Colloids Interfaces 2018, 2, 27; doi:10.3390/colloids2030027

Table 6. Core data for linear core floods

Experiment	Conc.	L (cm)	D (cm)	ϕ (-)	K_{wi} (Darcy)	K_{wf} (Darcy)	RRF (-)	η_i (cP)	η_e (cP)
No oil	500ppm	9.54	3.77	0.24	2.48	1.35	1.84	6.81	6.62
No oil	1500ppm	4.89	3.79	0.24	1.99	0.32	6.29	33.76	32.87
With oil, not aged	500ppm	10.44	3.78	0.23	1.83	0.36	5.08	6.65	6.77
With oil, aged	500ppm	9.85	3.78	0.23	2.27	0.27	8.41	6.99	5.90

Table 7. Core data for radial core floods

Experiment	Diameter (cm)	Thickness (cm)	Well radius (cm)	ϕ (-)	PV (ml)	Soi (frac)	Sorw (frac)	$K_{w,abs}$ (Darcy)	$K_{w,Sorw}$ (Darcy)	K_{wf} (Darcy)
No oil	30.00	2.20	0.15	0.24	373	n.a.	n.a.	2.600	n.a.	0.056
With oil	29.90	2.21	0.30	0.23	352	0.91	0.22	1.551	0.041	0.039

Figures

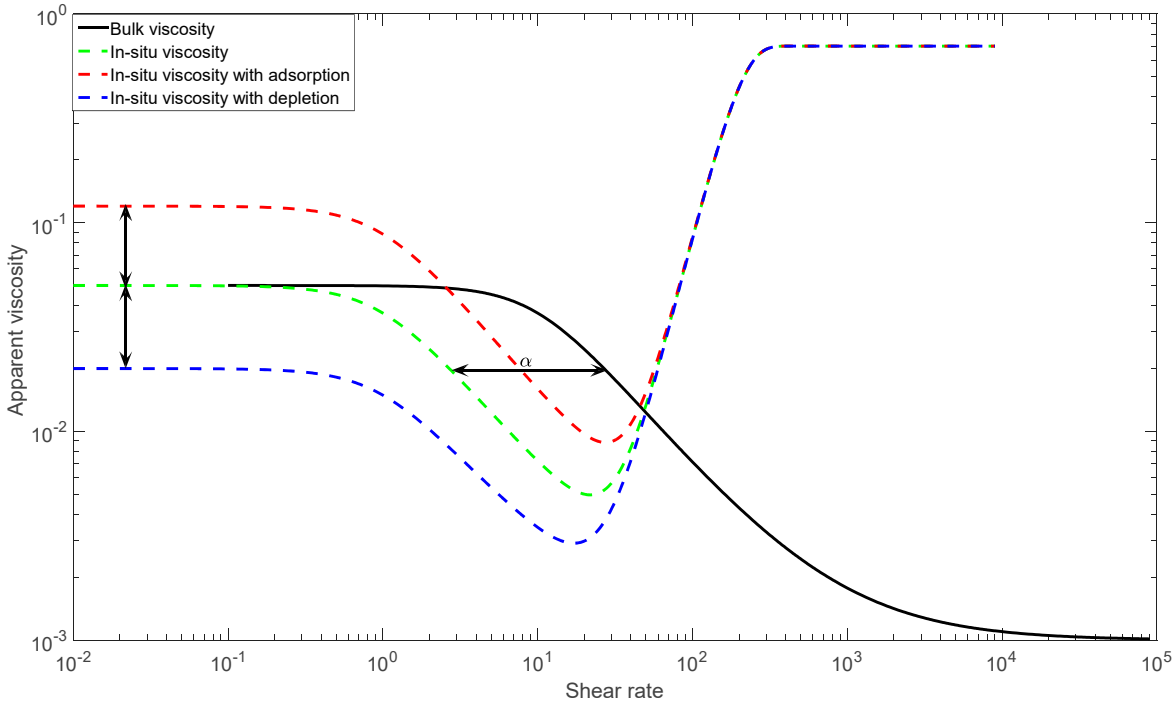

Figure 1: schematic comparison of in-situ and bulk rheology

Preprints (www.preprints.org) | NOT PEER-REVIEWED | Posted: 1 June 2018 doi:10.20944/preprints201806.0015.v1

Peer-reviewed version available at Colloids Interfaces 2018, 2, 27; doi:10.3390/colloids2030027

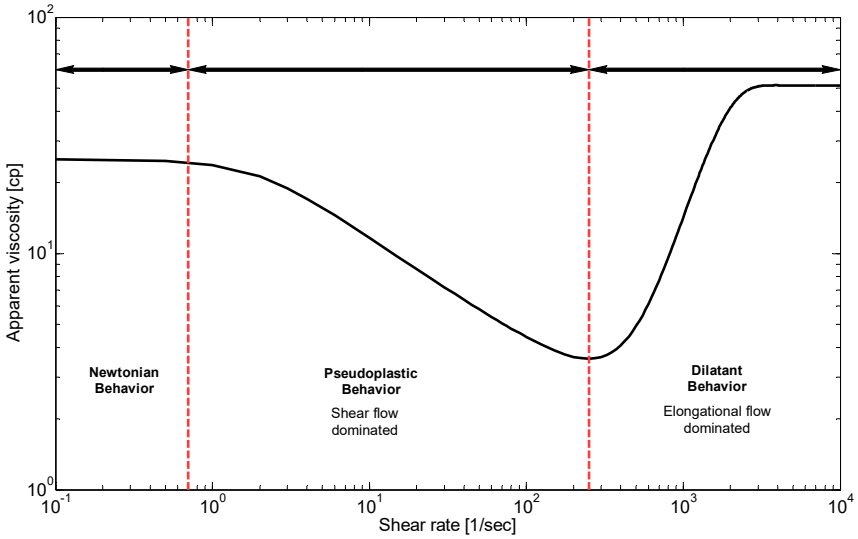

Figure 2 . Schematic illustration of apparent viscosity in porous media

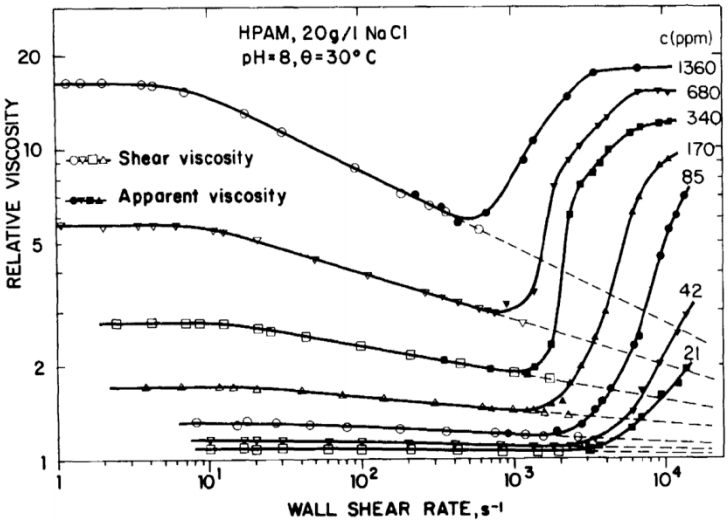

Figure 2: Effect of polymer concentration on the onset of extensional viscosity in a model with 45 successive constrictions[33]

Preprints (www.preprints.org) | NOT PEER-REVIEWED | Posted: 1 June 2018 doi:10.20944/preprints201806.0015.v1

Peer-reviewed version available at Colloids Interfaces 2018, 2, 27; doi:10.3390/colloids2030027

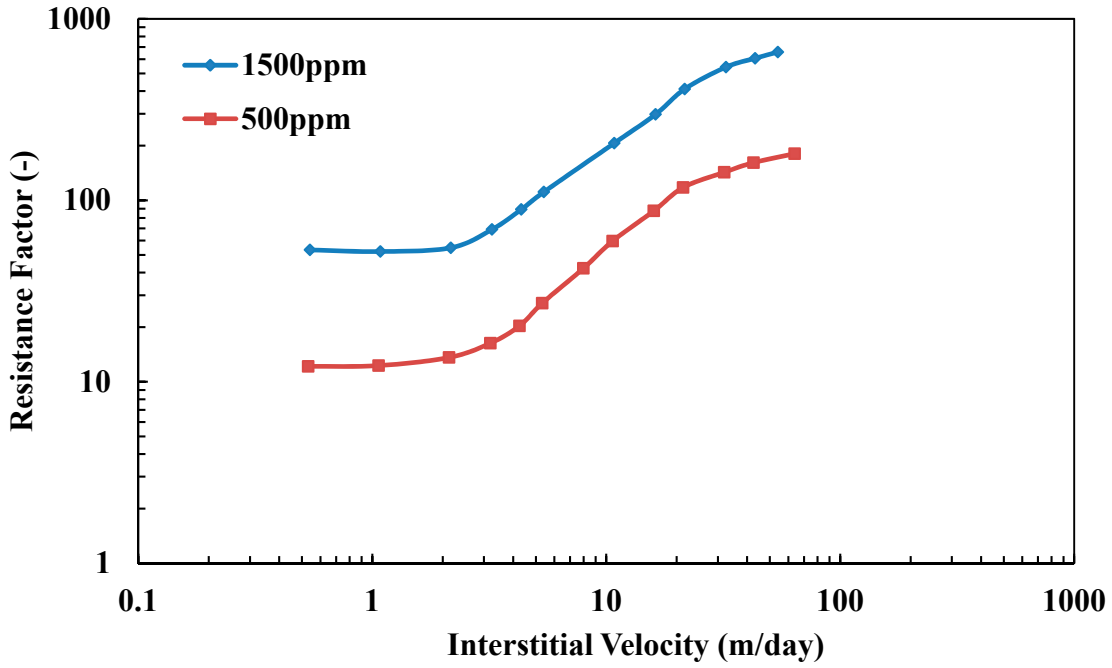

Figure 4 Resistance factor verse interstitial velocity of pre-filtered FP3630S HPAM polymer dissolved in 1 wt% NaCl brine.

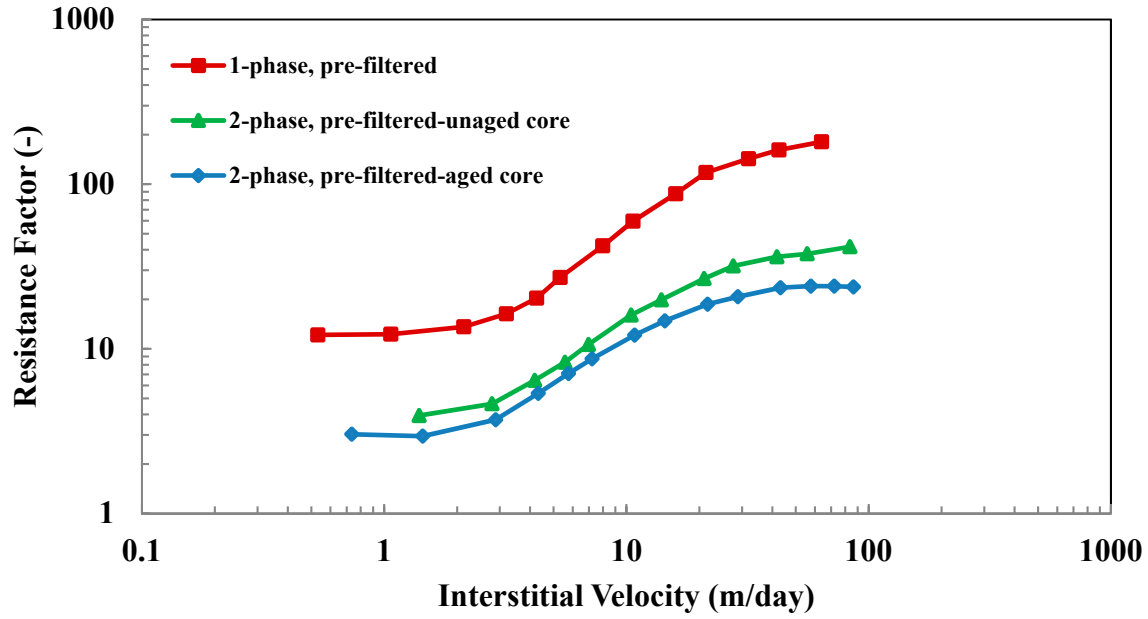

Figure 5: Resistance factor versus interstitial velocity of 500 ppm pre-filtered FP3630S HPAM polymer dissolved in 1 wt% NaCl brine, comparison of single phase polymer flow and polymer flow at residual oil saturation.

Preprints (www.preprints.org) | NOT PEER-REVIEWED | Posted: 1 June 2018 doi:10.20944/preprints201806.0015.v1

Peer-reviewed version available at Colloids Interfaces 2018, 2, 27; doi:10.3390/colloids2030027

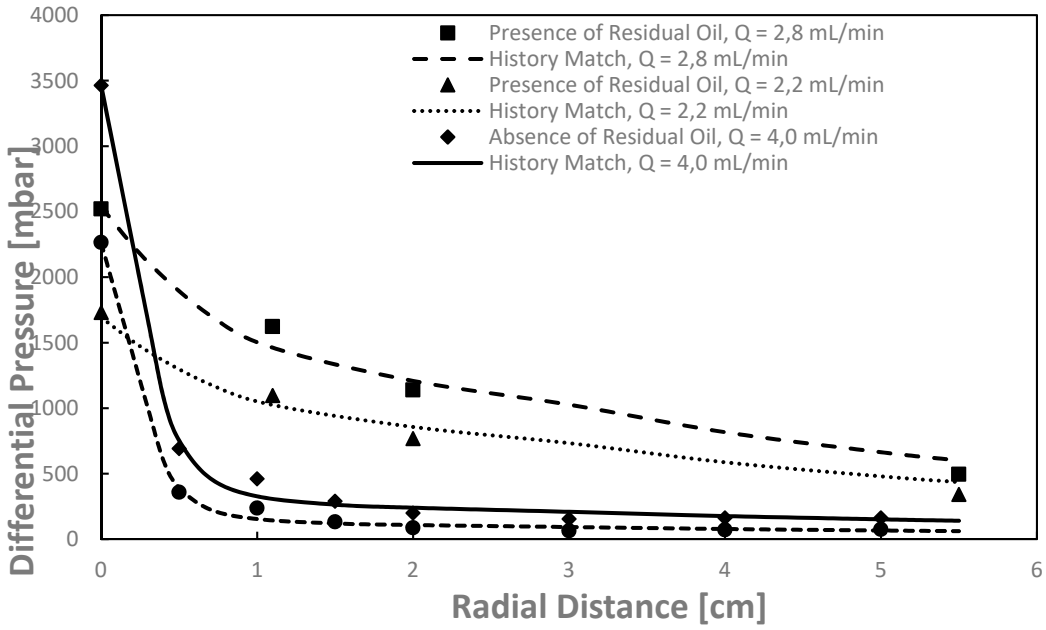

Figure 6: Differential pressure profiles for 800-ppm HPAM floods in presence and absence of residual oil in radial geometry as a function of distance from injector to producer for four flow rates.

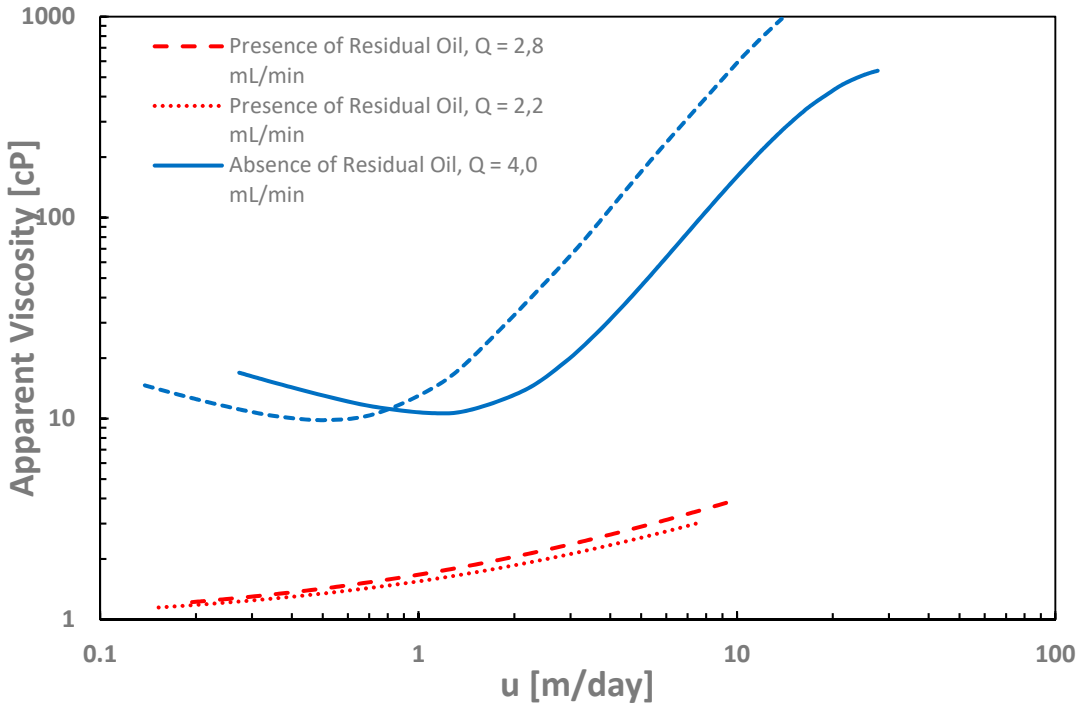

Figure 7: Apparent viscosity from history match of differential pressure for 800-ppm HPAM in presence and absence of residual oil in radial geometry.

Preprints (www.preprints.org) | NOT PEER-REVIEWED | Posted: 1 June 2018 doi:10.20944/preprints201806.0015.v1

Peer-reviewed version available at Colloids Interfaces 2018, 2, 27; doi:10.3390/colloids2030027

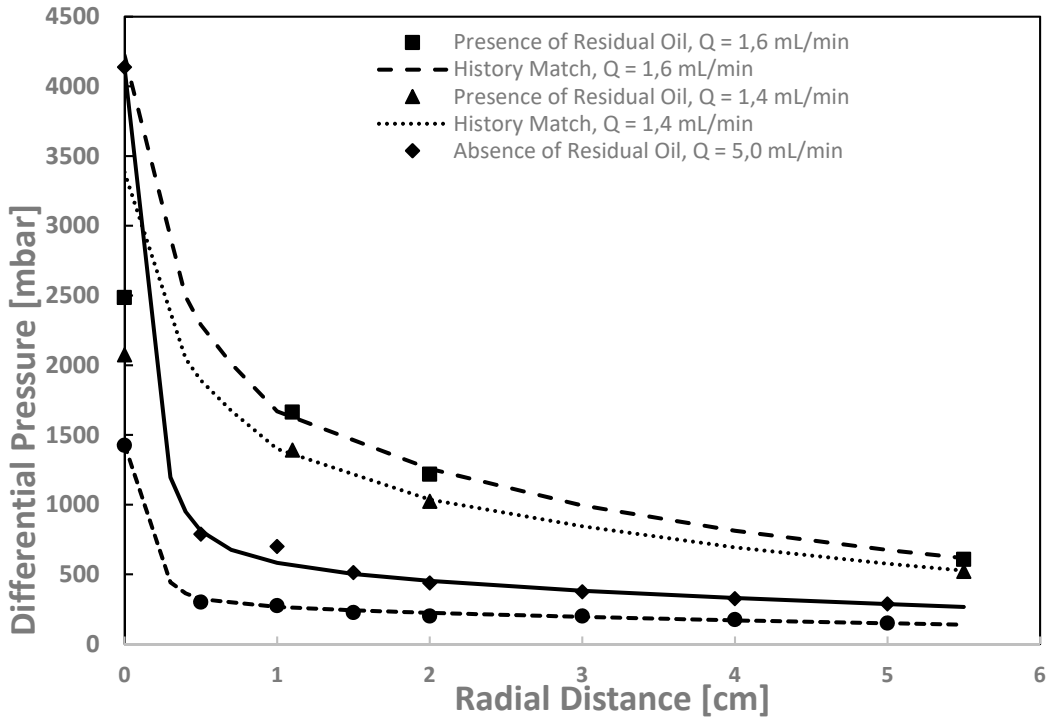

Figure 8: Differential pressure profiles for 2000-ppm 3630S HPAM floods in presence and absence of residual oil in radial geometry as a function of distance from injector to producer for four flow rates.

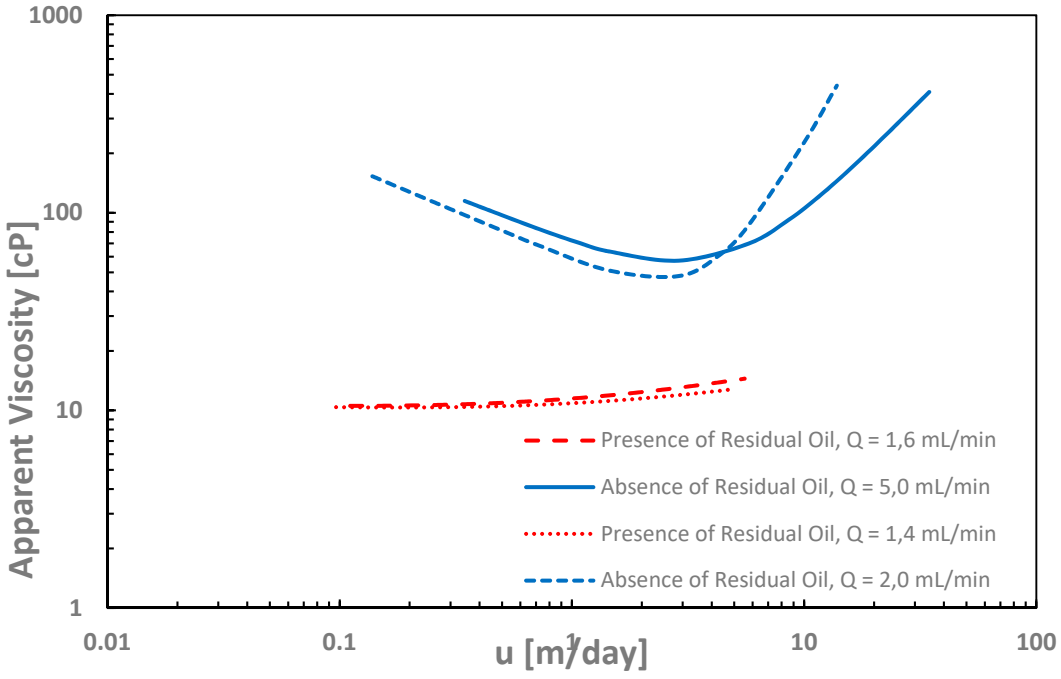

Figure 9: Apparent viscosity from history match of differential pressure for 2000-ppm 3630S HPAM in presence and absence of residual oil in radial geometry.